Article

Current Biology

Etiolated Seedling Development Requires Repression of Photomorphogenesis by a Small Cell-Wall-Derived Dark Signal

Graphical Abstract

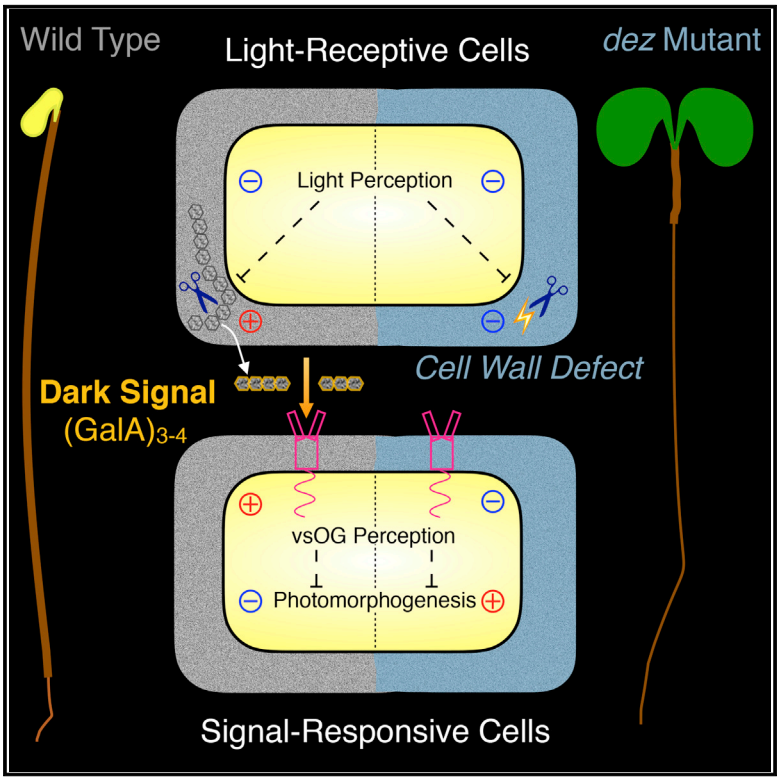

Authors

Scott A. Sinclair, Camille Larue, Laura Bonk, ..., Ulla Neumann, Michael J. Haydon, Ute Krämer

Correspondence

ute.kraemer@ruhr-uni-bochum.de

In Brief

Sinclair et al. report that several cell-wall-defective mutants mimic light-grown seedlings when grown in darkness, thus bypassing photoreception and subsequent signaling. Etiolated seedling growth can be restored by adding small fragments of the pectin homogalacturonan, suggesting their function as a dark signal in cell-cell communication.

Highlights

- Several cell-wall mutants mimic light-grown seedlings when grown in darkness
- Pectin-derived tri- and tetra-galacturonate restore normal dark-specific morphology
- Cell-wall signaling allows cell-cell communication in light-dependent development
- Accumulation of a plastid-derived oxylipin abolishes biogenesis of the dark signal

Sinclair et al., 2017, Current Biology 27, 3403–3418
November 20, 2017
https://doi.org/10.1016/j.cub.2017.09.063

Current Biology
Article

Etiolated Seedling Development Requires Repression of Photomorphogenesis by a Small Cell-Wall-Derived Dark Signal

Scott A. Sinclair,[1] Camille Larue,[1,6] Laura Bonk,[1,2] Asif Khan,[1] Hiram Castillo-Michel,[3] Ricardo J. Stein,[1,7] Daniel Grolimund,[4] Dominik Begerow,[2] Ulla Neumann,[5] Michael J. Haydon,[1,8,9,10] and Ute Krämer[1,8,11,*]
[1]Department of Molecular Genetics and Physiology of Plants, Ruhr University Bochum, Universitätsstrasse, 44801 Bochum, Germany
[2]Geobotany, Ruhr University Bochum, Universitätsstrasse, 44801 Bochum, Germany
[3]ID21 Beamline, European Synchrotron Radiation Facility, Avenue des Martyrs, 38043 Grenoble, France
[4]Swiss Light Source, Paul Scherrer Institute, 5232 Villigen PSI, Switzerland
[5]Central Microscopy, Max Planck Institute for Plant Breeding Research, Carl-von-Linné-Weg, 50829 Cologne, Germany
[6]Present address: ECOLAB, Université de Toulouse, CNRS, INPT, UPS, Avenue de l'Agrobiopole, 31326 Castanet Tolosan Cedex, France
[7]Present address: Faculdade Murialdo, Rua Marquês do Herval, 95020-260 Caxias do Sul-RS, Brazil
[8]Previous address: BIOQUANT Center, University of Heidelberg, Im Neuenheimer Feld, 69120 Heidelberg, Germany
[9]Previous address: Department of Biology, University of York, Wentworth Way, York YO10 5DD, UK
[10]Present address: School of BioSciences, The University of Melbourne, Royal Parade, Parkville 3010, Australia
[11]Lead Contact
*Correspondence: ute.kraemer@ruhr-uni-bochum.de
https://doi.org/10.1016/j.cub.2017.09.063

SUMMARY

Etiolated growth in darkness or the irreversible transition to photomorphogenesis in the light engages alternative developmental programs operating across all organs of a plant seedling. Dark-grown *Arabidopsis de-etiolated by zinc* (*dez*) mutants exhibit morphological, cellular, metabolic, and transcriptional characteristics of light-grown seedlings. We identify the causal mutation in *TRICHOME BIREFRINGENCE* encoding a putative acyl transferase. Pectin acetylation is decreased in *dez*, as previously found in the *reduced wall acetylation2-3* mutant, shown here to phenocopy *dez*. Moreover, pectin of *dez* is excessively methylesterified. The addition of very short fragments of homogalacturonan, tri-galacturonate, and tetra-galacturonate, restores skotomorphogenesis in dark-grown *dez* and similar mutants, suggesting that the mutants are unable to generate these de-methylesterified pectin fragments. In combination with genetic data, we propose a model of spatiotemporally separated photoreceptive and signal-responsive cell types, which contain overlapping subsets of the regulatory network of light-dependent seedling development and communicate via a pectin-derived dark signal.

INTRODUCTION

The irreversible transition from skotomorphogenic development in darkness to photomorphogenesis triggered by light is one of the most critical phases in the life cycle of a plant. Skotomorphogenesis in dark-grown ("etiolated") seedlings is characterized by an elongated hypocotyl and the maintenance of an apical hook that protects unopened cotyledons shielding the shoot apical meristem, while pro-plastid differentiation and root elongation are attenuated [1, 2]. This allows a newly germinated seedling to push through the soil, depending entirely on energy reserves stored in the seed. When the seedling perceives light, for example, in close proximity to the soil surface, photomorphogenic development ensues to realize a plant's inherent potential for photoautotrophic growth. This entails the arrest of hypocotyl elongation, the opening and growth of petioles and cotyledons, the differentiation of pro-plastids into chloroplasts, and root elongation.

Genes affecting light-dependent development were among the earliest identified in the model plant *Arabidopsis thaliana* [2]. Consequently, the associated cellular regulatory networks are mostly well understood [3]. In the dark, photomorphogenesis is suppressed through transcriptional repressors and multi-protein complexes mediating the proteolysis of transcriptional activators of light responses. Light-mediated activation of phytochrome red-light (PHY) and cryptochrome blue-light (CRY) photoreceptor proteins relieves the suppression of photomorphogenesis through initially parallel, but subsequently interacting, regulatory pathways.

Proteins required for the suppression of photomorphogenesis in the dark include CONSTITUTIVELY PHOTOMORPHOGENIC1 (COP1) and four partly redundant SUPPRESSOR OF PHYA (SPA) proteins interacting in ubiquitin E3 ligase complexes. COP10 and DE-ETIOLATED1 (DET1) act in a second multi-protein complex to activate ubiquitin-conjugating enzymes. Suppression of photomorphogenesis in the dark requires components of the COP9 signalosome, a multi-protein complex that interacts with both of these multi-protein complexes. Thus, the basic leucine zipper (bZIP) transcription factor ELONGATED HYPOCOTYL5 (HY5) is targeted for protein degradation among several additional photomorphogenesis-promoting transcriptional activators, whereas a

group of basic-helix-loop-helix (bHLH) transcription factors named PHYTOCHROME INTERACTING FACTORS (PIFs) are stabilized in the dark to repress photomorphogenesis [4]. Furthermore, PIFs integrate responses to phytochrome activation with phytohormone signaling, for example, via gibberellins and brassinosteroids [5].

Localized illumination of seedlings, excision of seedling organs and cell-type-specific expression of transgenes in wild-type and mutant backgrounds provided complementary lines of evidence for non-cell-autonomous responses to light during photomorphogenesis [1, 6, 7]. The molecular basis of the implied cell-cell communication, however, has not been identified. Transcript profiling revealed that photomorphogenesis is set apart from skotomorphogenic development through major cell-wall remodeling, among other processes [8]. For cells to expand during localized growth of either hypocotyls or cotyledons, cell walls must be loosened and new material deposited at an appropriate pace in order to exploit turgor pressure for directed expansion without allowing cells to burst [9]. Primary walls of *Arabidopsis* hypocotyl cells are composed of three major types of polysaccharides—cellulose, hemicellulose, and up to 35% pectin [10]. Of these, homogalacturonan constitutes the predominant proportion of about 65% of cell-wall pectin. Homogalacturonan consists of an unbranched chain of α-1,4-linked D-galacturonic acid (GalA) subunits that can carry chemical modifications of *O*-acetyl ester groups on C_2 and C_3 atoms (pectin acetylation) and methyl carboxyester groups on C_6 atoms of GalA subunits (pectin methylesterification). During the elongation of dark-grown hypocotyls, loosening is triggered in elongating cells by selective pectin de-methylesterification of longitudinal cell walls [11, 12]. Growth-associated cell-wall loosening involves a number of enzymatically mediated hydrolytic processes, which have the potential to release soluble oligosaccharide fragments from cell-wall polymers. Linear short oligogalacturonides (OGs) of 10–15 GalA subunits are cell-wall-integrity signals known also as elicitors of plant defenses against biotic stress [13, 14].

Here, we report photomorphogenesis in the dark that is enhanced under elevated zinc supply in the *de-etiolated by Zn* (*dez*) mutant. We identify the causal mutation at the *TRICHOME BI-REFRINGENCE* (*TBR*; At5g06700) locus [15], which encodes a member of the TBR-like (TBL) protein family implicated in *O*-acetylation of cell-wall macromolecules [16]. In darkness, *tbr* is epistatic or additive to most known mutants in the network controlling photomorphogenesis. Alterations in the transcriptome of *dez* are predominantly shared by characterized photomorphogenic mutants and are enriched in oxylipin/jasmonate signaling and photosynthesis transcripts. A GFP fusion of the TBR protein localizes to tri-cellular junctions of longitudinal cell walls. Cell-wall composition and cation binding of *dez*, combined with a similar photomorphogenic phenotype in a *reduced wall acetylation2* (*rwa2*) mutant, suggest that a primary reduction in pectin acetylation leads to increased pectin methylesterification and its sensitization to external Zn supply. Supplementation with very short OG fragments (vsOGs) restores skotomorphogenic development in *dez*, as well as in *rwa2* and two additional *dez*-phenocopying mutants, the cell-wall mutant *murus1* (*mur1*), and hormone biosynthesis mutant *jasmonate-resistant1* (*jar1*). This suggests that these mutants share with *dez* the lack of a cell-wall signal suppressing photomorphogenesis in the dark. We propose a model encompassing light-receptive cells spatiotemporally separated from photomorphogenesis-executing cells that respond to the elimination of a vsOG dark signal.

RESULTS

The *dez* Mutant Shows Photomorphogenesis in the Dark and Is Allelic to *tbr-1*

In a genetic screen for Zn-hypersensitive mutants, we identified an EMS mutant that showed characteristics of photomorphogenic development in the dark, including shortened hypocotyls, opened and enlarged cotyledons, and longer roots compared to the wild-type (Figure 1). We named this mutant *de-etiolated by zinc* (*dez*), because photomorphogenesis was enhanced on media supplemented with excess zinc (Zn), different from the previously described *constitutive photomorphogenesis* (*cop*) or *de-etiolated* (*det*) mutants [2]. Hypocotyls of *dez* seedlings cultivated on high-Zn media for 7 days in the dark were shortened, similar to those of the previously described *cop1-4* mutant [17] and slightly longer than hypocotyls of *det3* [18] (Figures 1A and 1B). Cotyledons of *dez* were opened less than those of *cop1-4* but far more widely than in *det3*. Similarly, roots of dark-grown *dez* were shorter than those of *cop1-4* but longer than roots of *det3*. Dark-grown *dez* seedlings contained higher amounts of chlorophyll than wild-type or *cop1-4* seedlings grown on the same high-Zn medium (Figure 1C; see STAR Methods). As another marker metabolite of light-triggered chloroplast differentiation [19], carotene contents of *dez*, but not of *cop1-4*, were higher than those of the wild-type. Plastids of dark-grown seedlings were larger in *dez* mutants and lacked the pro-lamellar body, a structure of paracrystalline tubule assemblies characteristic of etioplasts found in dark-grown wild-type seedlings (Figure 1D). This result is similar to previously reported observations in *cop1* and *det1* mutants, whereas plastid ultrastructure of dark-grown *cop2*, *cop3*, *cop4*, *det2*, and *det3* mutants resembled the wild-type [17, 18, 20–23].

Genetic mapping of *dez*, combined with the sequencing of candidate genes, identified a mutation in the *TBR* gene (see STAR Methods) [15, 24]. The *dez* mutant carries an intronic splice donor site G→A mutation that leads to the retention of the fourth intron in the mRNA (Figures S1A and S1B), thus resulting in an S→R amino acid exchange at position 491 of TBR, followed by several aberrant amino acids and a translational stop codon after position 496.

An allelic *tbr-1* mutant was previously reported to have altered cell-wall properties [15, 24]. A G→A mutation results in a G→E exchange at position 427 out of a total of 608 amino acids of the TBR protein of *tbr-1*, whereas the complete loss of *TBR* function was inferred to be lethal [24] (see Figure S1A). Both the *dez* and the *tbr-1* mutations are located within a conserved PC-esterase domain (PF13839 and IPR026057) that shares most, but not all, conserved residues with the GDSL/SGNH esterase protein superfamily [25]. When germinated under our growth conditions in the dark, *tbr-1* exhibited Zn-enhanced photomorphogenesis indistinguishable from that of *dez* (Figure S1C). A homozygous transgene encompassing the genomic region of the wild-type *TBR* gene translationally fused to GFP was able to phenotypically complement the *dez* mutant in both light and dark conditions (Figure S1D). Taken together, this demonstrates that

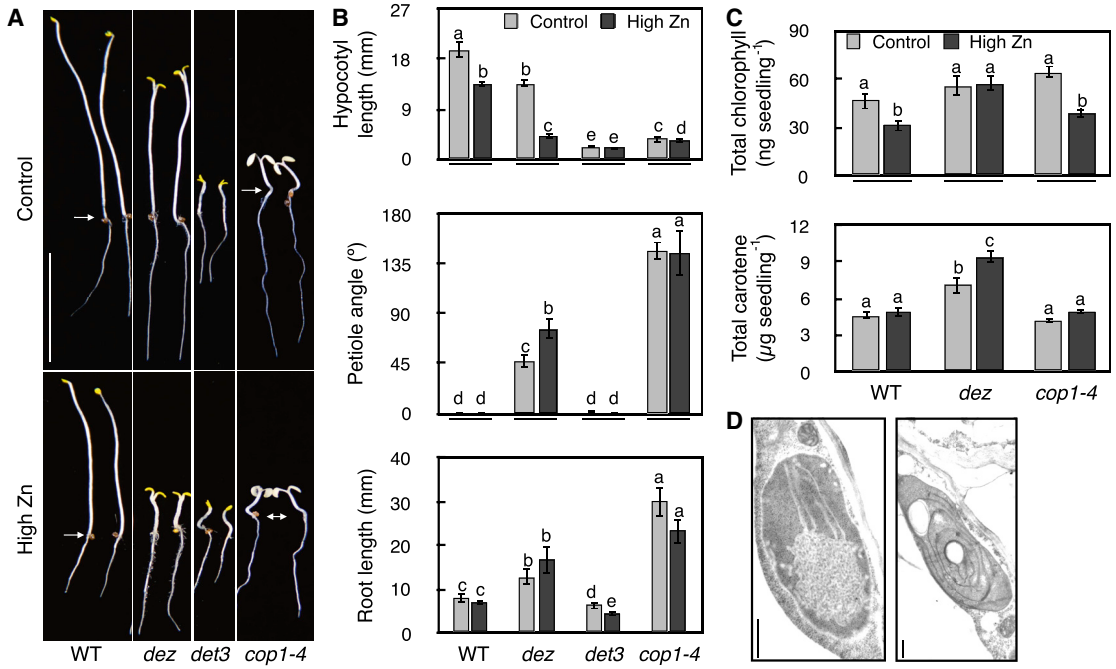

Figure 1. The *dez* Mutant Exhibits Zn-Enhanced Photomorphogenesis in the Dark

(A–C) Photographs (A) and quantification of morphological (B) and metabolic (C) markers of wild-type (WT) and mutant seedlings cultivated on control (5 μM Zn) and high-Zn (100 μM Zn) media in continuous darkness for 7 days. Arrows indicate root-hypocotyl junctions. Scale bars, 10 mm.

(D) Representative electron micrographs of a plastid in the cotyledon of high-Zn-grown WT (left) and *dez* (right) seedlings as shown in (A). Scale bars, 0.5 μm.

Bar graphs in (B) and (C) indicate arithmetic means ± SD (n = 8 replicate seedlings); different letters denote statistically significant differences (Student's t test with Bonferroni corrections; $p < 0.05$).

See also Figure S1 and Tables S1 and S2.

Zn-enhanced photomorphogenesis is caused by genetic lesions in the *TBR* gene.

Hypocotyl length of dark-grown *dez* seedlings decreased gradually with increasing Zn^{2+} concentrations in the medium, suggesting a quantitative physiological effect of Zn (Figure S1E). The *dez* mutant was hypersensitive to Zn in the light, with clear inhibition of root elongation, but not of hypocotyl elongation, when compared to the wild-type (Figures S1D and S1F). Supplementation of the medium with a moderately toxic concentration of Ni^{2+} also enhanced photomorphogenesis of dark-grown *dez* seedlings, but this was not found with the other tested metals, Ag^{+}, Cd^{2+}, Pb^{2+}, Co^{2+}, La^{3+}, Cu^{2+}, Fe^{III}HBED, Mg^{2+}, Mn^{2+}, and MoO_4^{2-}, or the chelators EGTA, CDTA, ferrozine, and EDTA (Figures S1G–S1J; Tables S1 and S2). However, photomorphogenesis was unique to *dez* among Zn-hypersensitive mutants (Figures S1K–S1N), namely, the *overly Zn-sensitive* mutants *ozs1* and *ozs2*, which are defective in the vacuolar membrane Zn^{2+}/H^{+} antiporter METAL TRANSPORT PROTEIN 1 (MTP1) and cell-wall-modifying PECTIN METHYLESTERASE 3 (PME3), respectively, and the *zinc-induced facilitator1* (*zif1*) mutant defective in the transport of the metal chelator molecule nicotianamine from the cytoplasm into the vacuole [26, 27].

Genetic Interactions with Known Loci Acting in Photomorphogenesis

By comparison to single *cop1-4* and *det1* mutants, *dez cop1-4* and *dez det1* double mutants were morphologically identical to *cop1-4* and *det1* in control conditions but showed additive phenotypes with respect to hypocotyl length under high-Zn conditions (Figures 2A, 2B, S2A, and S2B; for additional genotypes, see Table S3). In addition, we observed an increased production of anthocyanin in dark-grown *dez cop1-4* in high Zn (Figure S2A, bottom panel), reminiscent of the severe, seedling-lethal *cop1-5* mutant allele [28]. Several bHLH family PIF transcription factors act in the dark to repress photomorphogenesis [4]. As previously established, a dark-grown *pif1 pif3 pif4 pif5* (*pifq*) quadruple mutant exhibited a shortened hypocotyl and opened cotyledons under our growth conditions. Dark-grown quintuple *dez pifq* mutants were morphologically similar to *pifq* in control conditions but exhibited additive photomorphogenic phenotypes in high-Zn conditions (Figures 2C and S2C). The HY5 bZIP transcription factor protein acts directly to effect photomorphogenesis in the light, and it is subject to negative regulation through COP1 in the dark [29, 30]. In contrast to *hy5-215*, the hypocotyl length and petiole angle of the dark-grown *dez hy5-215* double mutant resembled those of the *dez* single mutant in both control and high-Zn media (Figures 2D and S2D). In the light, the *dez hy5-215* double-mutant hypocotyls were short under high-Zn conditions and elongated under standard growth conditions (Figures 2F and S2F). We concluded that the genetic interactions of *dez* with *cop1-4*, *det1*, *pifq*, and *hy5* are complex and Zn dependent. Under high-Zn conditions in darkness, *DEZ* either acts in parallel with, or is epistatic to, these regulators of photomorphogenic development.

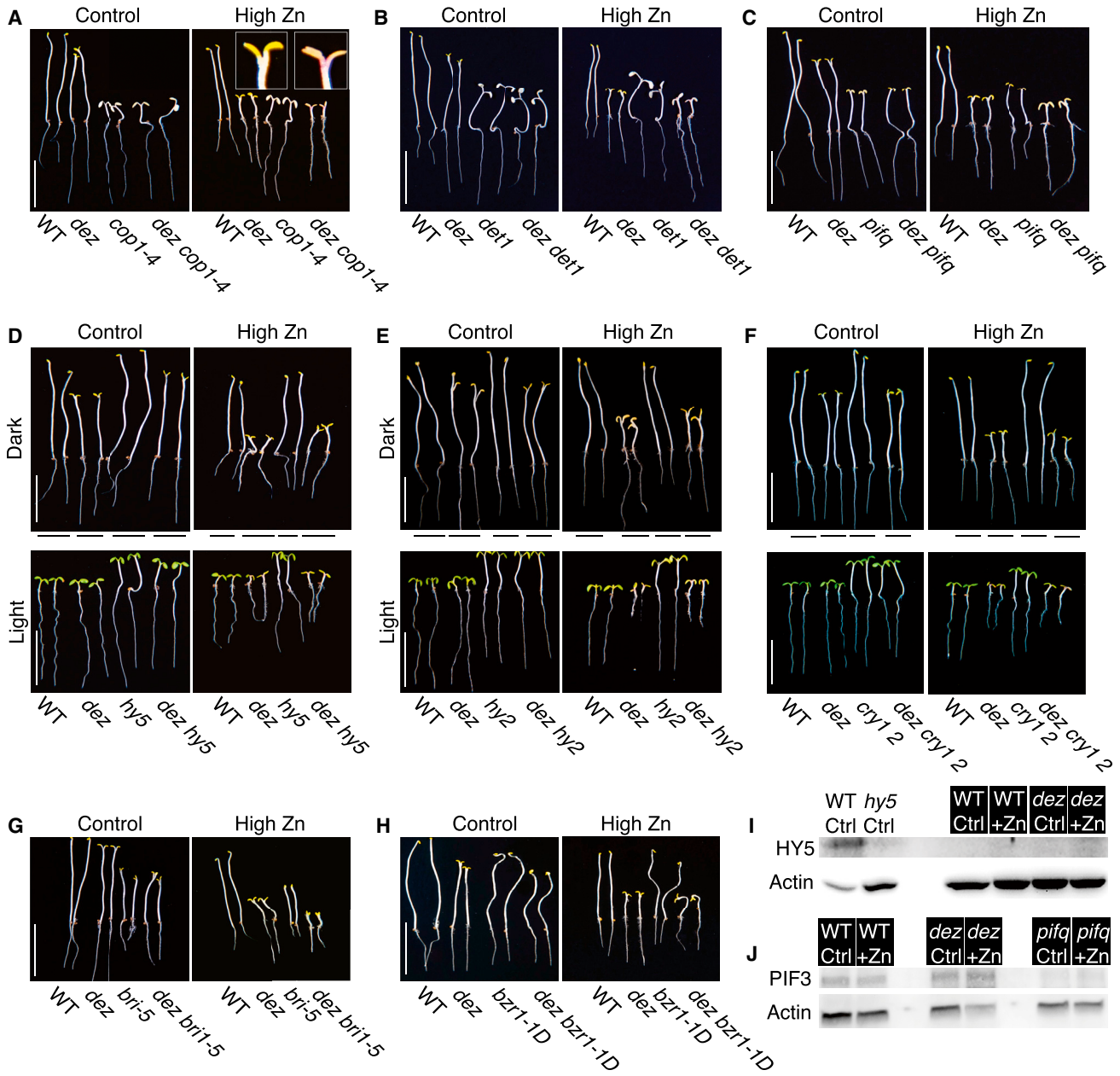

Figure 2. Conditional Epistasis of *dez* to Most Mutants Defective in Light-Responsive Development

(A–H) Photographs of wild-type (WT), *dez*, various mutants, and the respective *dez* double mutants cultivated on control (5 μM Zn) and high-Zn (100 μM Zn) media in (A–H) continuous darkness, and additionally in (D–F) light, for 7 days. Mutants and *dez* double mutants are: (A) *cop1-4* and *dez cop1-4*; (B) *det1* and *dez det1*; (C) *pifq* and *dez pifq*; (D) *hy5* and *dez hy5*; (E) *hy2* and *dez hy2*; (F) *cry1 cry2* and *dez cry1 cry2*; (G) *bri-5* and *dez bri-5*; and (H) *bzr1-1D* and *dez bzr1-1D*. Inset in (A) shows *dez* and *dez cop1-4* seedlings at higher magnification. Scale bars, 10 mm.

(I and J) Immunoblot detection of HY5 (I) and PIF3 (J) in total protein from 7-day-old seedlings cultivated on control and high-Zn media in continuous darkness (black background, white fonts), or in continuous light (black fonts).

See also Figure S2 and Tables S2 and S3.

Light activation of photoreceptors of red or blue light triggers photomorphogenic development. The function of all five phytochrome red-light photoreceptors of *Arabidopsis* depends on the covalently bound light-sensitive chromophore cofactor phytochromobilin. Consequently, *elongated hypocotyl 2* (*hy2*) mutants defective in phytochromobilin synthase display an elongated hypocotyl in white light and are skotomorphogenic in the dark [31, 32]. Dark-grown *dez hy2* seedlings were photomorphogenic as *dez* in both control and high Zn (Figures 2E and S2E). When germinated in the light, the *hy2* single mutant displayed an elongated hypocotyl in both high-Zn and control conditions. Hypocotyl length of light-grown *dez hy2* seedlings was *dez*-like in high Zn but *hy2*-like in standard growth medium. Similar observations were made for *cry1 cry2* defective in the

blue light photoreceptors acting in photomorphogenesis (Figures 2F and S2F). Our results suggested that *DEZ* is epistatic to the phytochrome and cryptochrome photoreceptors under control and high-Zn conditions (see Table S3 for additional light conditions).

Several phytohormones have been implicated in the transition from skotomorphogenesis to photomorphogenesis [5]. Growth on media supplemented with various hormone agonists and antagonists did not reveal any noteworthy hormonal effects on the *dez* phenotype (Table S2). The brassinosteroid signaling pathway is of particular interest in this context, because it was implicated in both cell-wall signaling [33] and photomorphogenesis. Therefore, *dez bri1-5* and *dez bzr1-1D* mutants were generated to inactivate and constitutively activate brassinosteroid signaling, respectively, in the *dez* background. Both double mutants phenotypically resembled *dez* in high Zn in the dark, suggesting independence of the effects of *dez* mutation from brassinosteroid signaling (Figures 2G, 2H, and S2G–S2J; see also Table S3). Roles for sucrose were discussed in root elongation during photomorphogenesis [34] and in the suppression of phyA-mediated responses to far-red light [35]. Zn-enhanced photomorphogenesis of *dez* seedlings remained on media lacking sucrose (Table S2). HY5 protein was undetectable and PIF3 protein was detectable in both *dez* and wild-type seedlings grown in the dark in control and high-Zn media (Figures 2I and 2J).

Altered Abundance of Cell-Wall-, Light-Signaling- and Wounding-Related Transcripts in *dez*

To gain information on the molecular alterations contributing to the *dez* phenotype, we conducted transcriptome profiling of 7-day-old wild-type and *dez* seedlings cultivated in the dark on control and high-Zn media. The majority of transcripts de-regulated in *dez* and previously reported as light regulated showed congruent alterations in both the *det1* and *pifq* photomorphogenic mutants (Figures 3A and 3B) [8, 36], for example *PMEpcrD* (*At2g43050*) encoding a pectin methylesterase (PME) with a PME inhibitor domain, *INDOLE-3-ACETIC ACID6* (*IAA6*)/*SHORT HYPOCOTYL1* (*SHY1*), and *ARABINOGALACTAN PROTEIN4* (*AGP4*, *JAGGER*), or in only one of these mutants, for example *PHYTOCHROME RAPIDLY REGULATED1* (*PAR1*) and *DARK-INDUCIBLE10* (*DIN10*) (see Data S1 for more information). Transcript levels of these genes were generally lower in *dez* than in the wild-type, and this was more pronounced under high-Zn conditions, as confirmed by qRT-PCR (Figures S3A–S3E).

Parametric analysis of gene set enrichment (PAGE) suggested a prominent de-regulation of cell-wall biosynthesis, modification, and signaling, as well as of jasmonate (JA)/oxylipin biosynthesis and responses, in *dez* seedlings (Figures 3C and 3D). The corresponding genes included, for example, *PMEpcrD*, *AGP4*, the xyloglucan endotransglucosylase/hydrolase-encoding *TOUCH4* (*TCH4*), *BETA-XYLOSIDASE1* (*BXL1*), *WALL-ASSOCIATED KINASE1* (*WAK1*), related to the cell wall; and *RESPIRATORY BURST OXIDASE HOMOLOG D* (*RBOHD*), *LIPOXYGENASE2* (*LOX2*) and *OXOPHYTODIENOATE-REDUCTASE3* (*OPR3*), related to JA signaling and biosynthesis (Figures S3A, S3C, and S3F–S3K; Data S1). In addition, plastid stroma-related functions were over-represented among differentially abundant transcripts in the *dez* mutant by comparison to the wild-type under high-Zn conditions. Among these genes were *GLUTAMYL-TRNA REDUCTASE* (*HEMA1*), *PHOTOSYSTEM I LIGHT HARVESTING COMPLEX GENE1* (*LHCA1*), *CARBONIC ANHYDRASE1* (*CA1*), or the proposed target of positive regulation by HY5, *CHLOROPHYLL A/B BINDING PROTEIN1* (*CAB1*) (Figures S3L–S3O; Data S1). Transcript levels of most of these genes were de-regulated in the *dez* mutant either fully (*HEMA1*) or partially (*LHCA1*, *CAB1*) and congruent with both light-dependent regulation and alterations in *hy5*, *pifq*, and *det1* [8, 22]. In summary, gene expression in the *dez* mutant is consistent with morphological data (see Figure 1), and it implicates cell-wall remodeling, JA/oxylipin signaling, and alterations in plastid processes in the *dez* phenotype.

Decreased *O*-Acetylation and Increased Zn-Sensitized Methylesterification of Pectins in *dez*

TBR was hypothesized to act in the chemical modification of cell-wall pectin by *O*-acetylation of the hydroxyl groups of C_2 and C_3 of galacturonic acid subunits [16, 24, 25]. The *O*-acetylation of cell-wall macromolecules occurs in the lumen of the Golgi [25]. Indeed, a large-scale proteomic study identified TBR among Golgi luminal proteins at low abundance in two out of four independent experiments [37], whereas another similar study did not identify TBR among many other Golgi-localized cell-wall-modifying proteins [38]. In *dez* transgenic lines homozygous for a complementing translational GFP fusion construct of *TBR* under the control of its own promoter (see Figure S1D), we detected GFP fluorescence exclusively in the apoplast of both roots of light-grown and hypocotyls of dark-grown seedlings (Figures 4A, 4B, and S4A). There was no apparent Zn-dependent (data not shown) or light-dependent change in localization or intensity of GFP fluorescence. GFP fluorescence was restricted to longitudinal cell walls at tricellular junctions and small regions of peripheral cell walls of the hypocotyl epidermis. Despite this result, we cannot exclude the localization of a minor fraction of TBR-GFP fusion protein to the Golgi.

Micro-Fourier-transformed infra-red (μFTIR) spectra of transverse sections of dark-grown freeze-dried hypocotyls suggested pronounced overall differences between *dez* grown in high-Zn medium and all other samples (Figure 4C). Spectra were most consistent with predominant alterations in pectin (peaks 1 to 6) and pectin modifications, namely, pectin methylesterification (peaks 8, 10, and 12) and pectin acetylation (peaks 3 and 4), among possible changes in various other cell-wall components, given the complexity of the samples and obtained spectra (Figure 4D; Table S4).

The biochemical analysis of pectin modification in dark-grown seedlings confirmed reduced levels of pectin acetylation in *dez* to between 51% and 69% of the wild-type (Figure 4E). This is consistent with a role for TBR in either the catalytic transfer of acetyl groups onto pectin in the lumen of the Golgi or the protection of *O*-acetylated pectin from de-acetylation by pectin acetyl esterases in the cell wall [25, 39], the latter concurring with the extracellular localization of the TBR-GFP protein (see Figures 4A and 4B). Plant pectins are synthesized in methylesterified form in the Golgi lumen and secreted into the apoplast, where PMEs can release methanol to generate free C_6 carboxyl groups

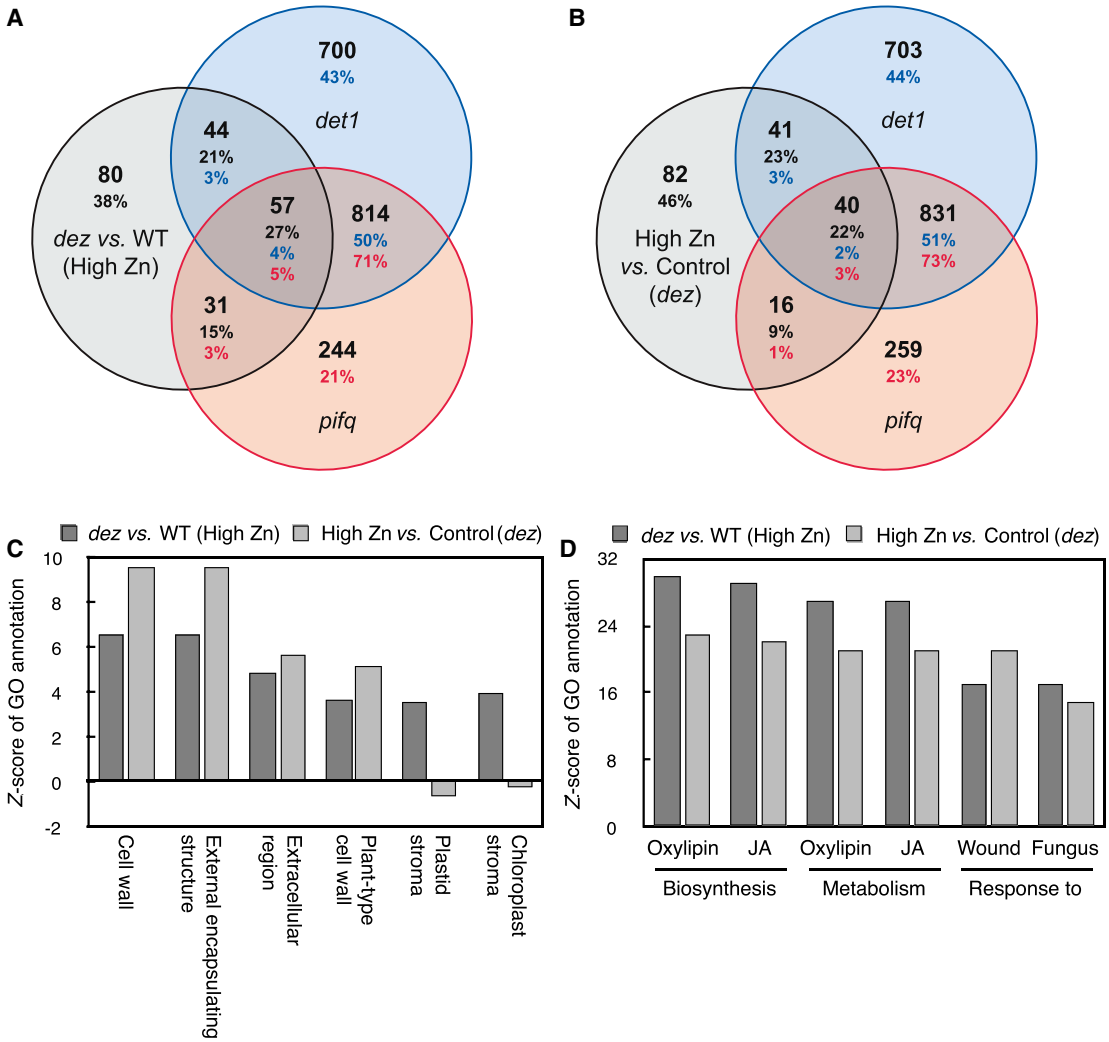

Figure 3. Transcriptome Changes in *dez* Are Consistent with Photomorphogenesis

(A and B) Venn diagrams visualizing the overlap between transcripts de-regulated in *dez* compared to the wild-type (WT) under high-Zn conditions (A), or between transcripts exhibiting a Zn-dependent change in abundance in *dez* (B), and transcripts published as de-regulated in *det1* and *pifq* mutants [8], among light-regulated transcripts. Only genes showing a congruent directional change in transcript levels were scored as overlapping.

(C and D) The top six over-represented GO Annotations for Cellular Component (C) and for Biological Process (D) according to parametric analysis of gene set enrichment (PAGE). Positive/negative *Z* scores show significant over/under-representation (Hochberg multiple testing adjustments in PAGE; $p < 0.05$). Fold changes of all entities were determined in 7-day-old *dez* versus wild-type seedlings at 100 μM Zn and in *dez* seedlings at 100 μM versus 1 μM Zn.

See also Figure S3 and Data S1.

on the galacturonic acid residues of pectin macromolecules. Overall, cell walls of dark-grown *dez* seedlings exhibited a 1.75-fold increase in pectin methylesterification compared to the wild-type, and this was enhanced by an additional 20% in seedlings grown under high-Zn conditions (Figure 4F; compare with Figure S4B). Enhanced pectin methylesterification in high-Zn-grown *dez* was accompanied by increased—rather than decreased—net endogenous PME activity (Figure 4G), suggesting a spatial separation between PME activity and its substrates.

While the imaging of *O*-acetylated pectins is not possible, specific antibodies are available for assessing the degree of methylesterification of homogalacturonan, the predominant form of pectin in *Arabidopsis* hypocotyls [40]. In agreement with our biochemical data, immunogold staining of sections through the midpoint of the hypocotyl of dark- and high-Zn-grown seedlings indicated an increased relative abundance of methylesterified pectin at tri-cellular junctions and surrounding epidermal cells of *dez* in comparison to the wild-type (Figures 4H–4J). Thus, we propose that these cell-wall domains, which corresponded to the sites of TBR-GFP protein localization in the wild-type, were less accessible to endogenous PMEs in the *dez* mutant than in the wild-type in both control and high-Zn media (Figures S4C and S4D). For example, an about 5-fold increase in cell-wall thickness may have overcompensated the increase in PME activity through a dilution-like effect, to result in a more strongly enhanced degree of pectin methylesterification in high-Zn-grown *dez* seedlings, compared to the wild-type (Figures 4G–4K, S4C, and S4D).

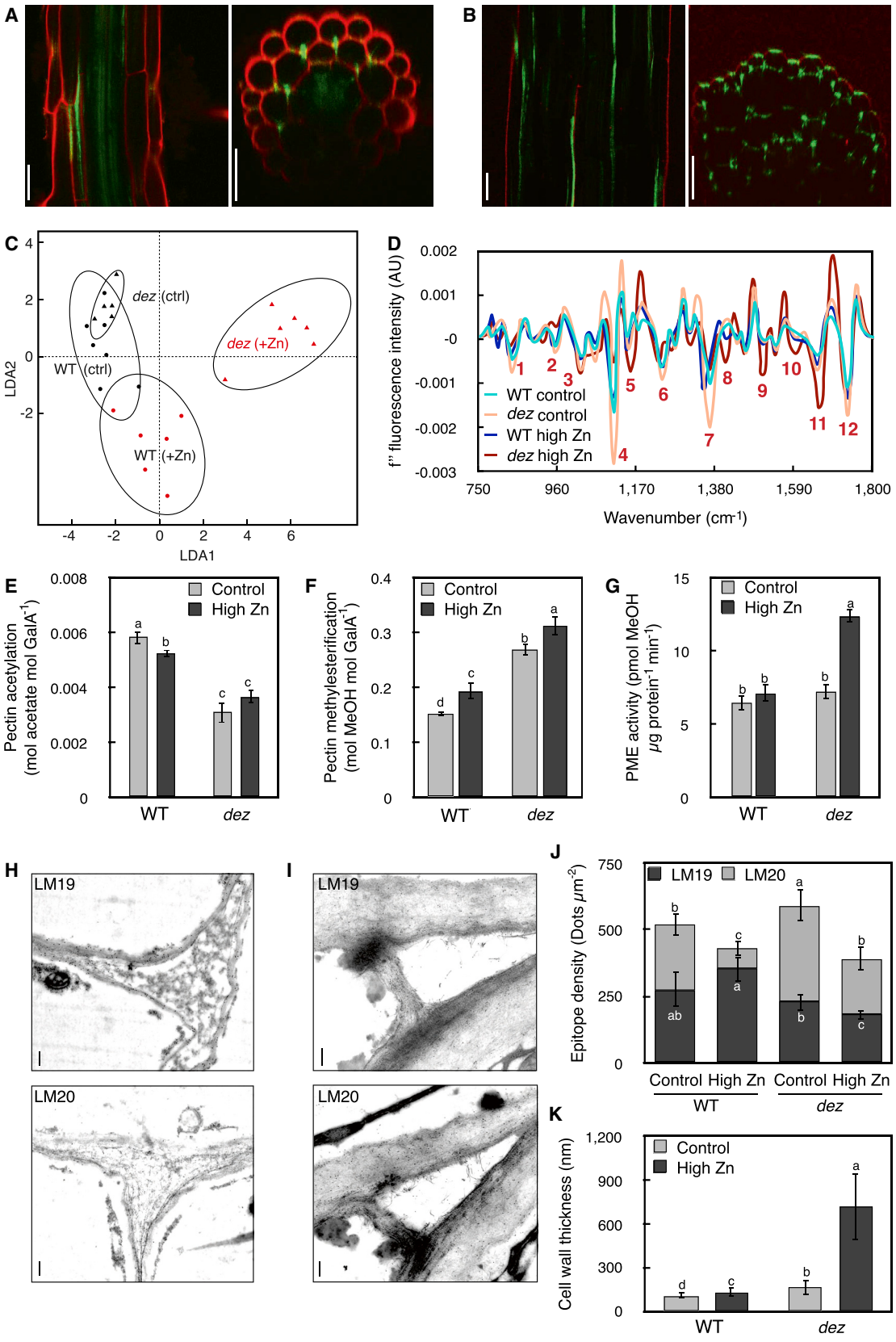

(legend on next page)

A predicted consequence of altered pectin modification of *dez* is a change in cell-wall cation-binding properties, because de-methylesterification of homogalacturonan forms free carboxyl groups, which can act as high-affinity binding sites of divalent cations, particularly Ca^{2+} [41]. Indeed, comparative element analysis of untreated and desorbed seedlings, in which easily accessible cell-wall cations had been removed in a solution containing metal chelator, indicated that *dez* seedlings grown in high Zn have a lower capacity to retain divalent Zn^{2+} cations in the cell wall than the wild-type (Figure S4E). Moreover, high-Zn-grown *dez* seedlings accumulated less Ca in both the total fraction and the extracellular fraction that was removed by desorbing. Micro-X-ray fluorescence spectroscopy (μXRF) of transverse hypocotyl cryo-sections suggested a similar spatial distribution of Zn^{2+} and Ca^{2+} in both wild-type and *dez* seedlings (Figures S4F and S4G). According to micro-X-ray absorbance near-edge spectroscopy (μXANES) analysis, the predominant proportion of Zn^{2+} was bound to pectin in the wild-type. In contrast, Zn binding was less uniform in *dez*, with best fits for bulk cell-wall material rather than a purified pectin fraction, in combination with thiol binding and sometimes other model compounds (Figures S4H and S4I). Taken together, our results suggest that the ease of dissociation of cell-wall-bound Zn^{2+} in *dez* can be explained by substantially reduced amounts of carboxylate groups of de-methylesterified pectin in the cell wall.

Phenotypic Rescue of Photomorphogenesis in Dark-Grown *dez* and Other Mutants by the Addition of Very Short Oligogalacturonides

To gain additional insights into how photomorphogenic development arises in *dez*, we examined other mutants in cell wall and JA biosynthesis, based on the transcriptome of the *dez* mutant (see also Table S3). The *prc1-1* mutant, a loss-of-function allele of the gene encoding cellulose synthase isoform CESA6, developed a shortened hypocotyl, as reported earlier [42], but cotyledons did not open (Figure 5A, upper panel). This suggested that *prc1-1* is merely defective in cell elongation in the dark and not constitutively photomorphogenic. By contrast, the cell-wall mutants *rwa2-3* and *mur1-2* were phenotypically more *dez*-like. RWA2 contributes to the transport of acetyl-coenzyme A (CoA) into the Golgi where cell-wall polysaccharides are *O*-acetylated, and the degree of *O*-acetylation of both pectins and xyloglucans is reduced by 20% in the *rwa2-3* mutant [25, 43, 44]. The *O*-acetylation step itself is thought to be carried out by RWA proteins themselves or by a TBL family protein. The *rwa2-3* mutant exhibited photomorphogenesis in the dark when cultivated on high-Zn media, yet less severely than *dez* (Figure 5A, upper panel). *MUR1* encodes a GDP-D-mannose-4,6-dehydratase that is required for the first step of fucose biosynthesis. In the cell wall of *mur1-2* mutants, both hemicellulose and pectin fractions are deficient in fucose, resulting in less than 2% of the wild-type fucose content [45]. In contrast to the other mutants, *mur1-2* showed characteristics of photomorphogenesis in the dark equally under control and high-Zn conditions (Figure 5A, upper panel). In support of a causal role of pectin alterations in photomorphogenic development, the *mur2* mutant defective in a xyloglucan fucosyltransferase [46] exhibited skotomorphogenesis in the dark indistinguishable from that of the wild-type (Table S3). Finally, out of a number of JA biosynthetic and signaling mutants examined (see Figure 3), only *jar1* mutants defective in the final JA-isoleucine conjugation step that forms the signaling-active form of JA phenocopied *dez* (Figure 5A; Table S3; see also Figure S6).

We hypothesized that the photomorphogenic phenotype of *dez* results from the disruption of an extra-cellular suppressive signal, which acts in wild-type seedlings to maintain skotomorphogenesis in the dark. Based on the cell-wall modifications observed in *dez*, such a signal could be a wall-derived OG signal. To test this, we asked whether supplementation of growth media with a crude enzymatic digest of polygalacturonic acid (PGA) restored skotomorphogenesis in the dark in *dez* and other mutants. Indeed, this was observed for *dez*, *rwa2-3*, *jar1-1*, and *mur1-2*, as quantified by both hypocotyl length and petiole angle (Figures S5A and S5B). Importantly, the Zn hypersensitivity of light-grown *dez* seedlings persisted in the presence of the PGA digest, indicating that the digest did not act by merely reducing the bioavailability of Zn in the growth medium (Figures S5C and S5D), despite the ability of both PGA and OG (degree of polymerization [DP] $\geq$ 10) to bind Zn [47]. Supplementation with the PGA

Figure 4. Extracellularly Localized TBR/DEZ Protein Is Required for Pectin Modification and Cell-Wall Architecture

(A) Confocal laser scanning microscopic images of roots of 7-day-old light-grown *dez* transformant seedlings homozygous for a genomic *TBR* fragment (1,615 bp upstream and coding region) translationally fused to *GFP*. Images of GFP (green) and propidium iodide (red) in the longitudinal (left) and transverse (right) planes. Scale bars, 50 μm.

(B) Same as in (A) for hypocotyls of dark-grown seedlings.

(C) Principal-component linear discriminant analysis (PCLDA) of μFTIR spectra. Each data point represents a transverse hypocotyl section of one 7-day-old dark-grown seedling (triangles indicate *dez*; circles indicate WT; red symbols indicate 100 μM Zn; and black symbols indicate 1 μM Zn). Ovals delineate 95% confidence intervals using PC1 to PC5.

(D) μFTIR spectra of *dez* mutant and wild-type hypocotyls. Shown are means (n ~6); see (C). Numbered peaks contribute to PC2, the predominant component of PCLDA1 and, thus, of the differences between *dez* at high Zn and all other treatments and genotypes (see Table S4 for peak assignment).

(E and F) Degree of pectin acetylation (E) and methylesterification (F) in 7-day-old dark-grown wild-type and *dez* seedlings cultivated in control (5 μM Zn) and high-Zn (100 μM Zn) media.

(G) Pectin methylesterase (PME) activity quantified in vitro using total protein extracts from seedlings; see (E).

(H and I) Electron micrographs of tri-cellular junctions in transverse sections of the hypocotyls of 7-day-old dark-grown wild-type (H) and *dez* mutant (I) seedlings cultivated in high-Zn media. Black dots correspond to immuno-gold labels obtained with LM19 (top) and LM20 (bottom) antibodies. Scale bars, 0.2 μm in (H) and 1 μm in (I).

(J and K) Quantification of immunogold labels (J) and cell-wall thickness (K) observed (see H, I, and Figures S4C and S4D).

Bar graphs indicate arithmetic means ± SD (n = 4 subsamples from a pool of 140 to 160 seedlings in E–G, n = 8 images in J, and n = 18 images in K); different letters denote statistically significant differences (Student's t test with Bonferroni corrections; $p < 0.05$).

See also Figure S4 and Tables S2, S3, and S4.

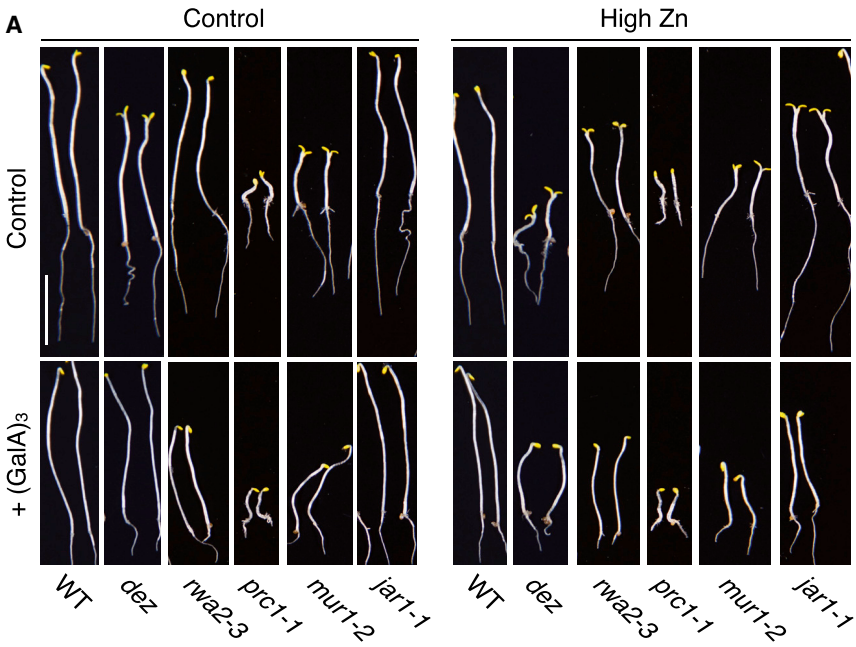

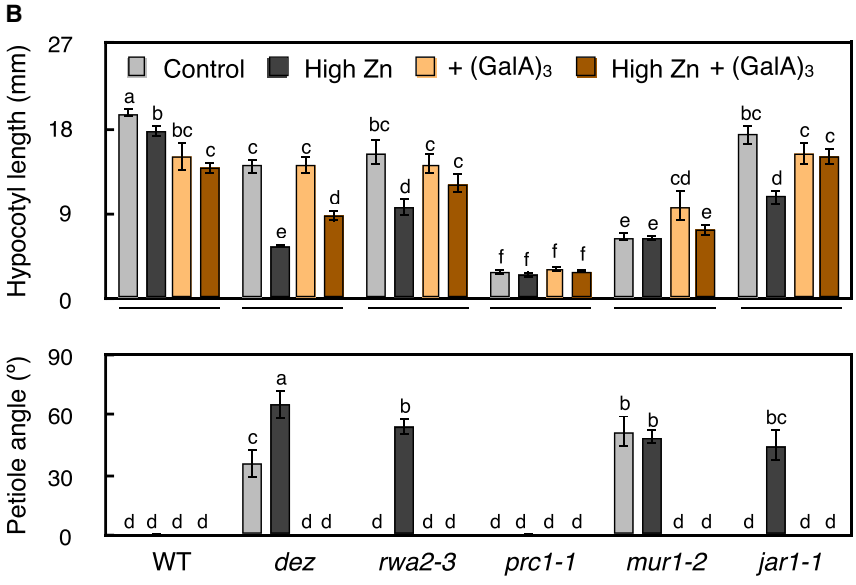

Figure 5. Photomorphogenesis in Darkness in *dez*, *rwa2, mur1*, *and jar1* and Mutants and Its Rescue by Tri-galacturonate

(A and B) Photographs (A) and quantification of morphological markers (B) of 7-day-old dark-grown wild-type (WT) and mutant seedlings cultivated on control (5 μM Zn) and high-Zn (100 μM Zn) media without and with 500 μM tri-galacturonic acid ($(GalA)_3$). Scale bar, 10 mm.

Bar graphs indicate arithmetic means ± SD (n = 8 replicate seedlings); different letters denote statistically significant differences (Student's t test with Bonferroni corrections; $p < 0.05$).

See also Figure S5 and Tables S2 and S3.

digest did not have a significant effect on the photomorphogenic mutants *cop1-4* and *pifq*, but it decreased the extent of cotyledon opening in *det1* (Figures S5A and S5B). OGs were reported to inhibit growth [13, 48], and this was also observed in both light- and dark-grown seedlings through an inhibition of root growth (Figures S5A–S5D). Given that skotomorphogenesis was restored in *dez* by a digest of PGA, which constitutes the simple, chemically unmodified backbone of homogalacturonan, we next tested the galacturonic monomer and oligomers of increasing lengths (Table S2). Indeed, tri- and tetra-galacturonic acid ($(GalA)_3$ and $(GalA)_4$) were able to rescue the photomorphogenic phenotypes of dark-grown *dez* as well as *rwa2-3*, *mur1-2*, and *jar1-1* (Figures 5A, lower panel, and 5B; Table S2). $(GalA)_3$ did not rescue *cop1*, *pifq*, or *det1* mutants in the dark, and it also did not rescue Zn hypersensitivity of light-grown *dez* seedlings (Figures S5E–S5G). This is consistent with a lack in *dez*, *rwa2-3*, *mur1-2*, and *jar1-1* of a very short OG (vsOG) dark signal that is necessary and sufficient to maintain skotomorphogenesis in darkness.

Positioning of *dez* and *dez*-Like Mutants in the Regulatory Network Governing Light-Dependent Development

Photomorphogenesis in *jar1-1* and the allelic *jar1-11* mutant (see Table S3), as well as the *dez* transcriptome, implicated JA/oxylipin signaling (see Figure 3). Indeed, the addition of methyl JA to our media led to a small extent of photomorphogenic development in dark-grown wild-type and *dez* seedlings (Table S2). A *dez jar1-1* double mutant established that both mutations were not additive, with dark grown *dez jar1-1* seedlings resembling *dez* in high Zn (Figures 6A and 6B), consistent with JAR1 acting upstream of *dez*. To test whether the effect of *jar1* arose through the accumulation of a biosynthetic intermediate of the JA pathway upstream of JAR1 [49], we tested *jar1-1 aos* [50] and *jar1-1 opr3* double mutants. AOS and OPR3 catalyze early steps in the biosynthetic pathway of JA, namely, the synthesis and processing, respectively, of the precursor molecule 12-oxo-phytodienoic acid (OPDA), for which independent signaling roles have been proposed [51, 52]. In confirmation of our hypothesis, dark-grown *jar1-1 aos* seedlings were skotomorphogenic in the dark just like the wild-type in both control and high-Zn conditions (Figures 6A and 6B). By contrast, the persistence of photomorphogenic development in *jar1-1 opr3* suggested that allene oxide, one of its spontaneous hydrolysis products, or an OPDA isomer is required for triggering photomorphogenesis in dark-grown *jar1-1*. Interestingly, however, both *dez aos* and *dez opr3* double mutants, as well as the *dez coi1-16* double mutant impaired in the perception of JA-Ile, all resembled *dez* in high Zn in the dark (Figures S6A and S6B).

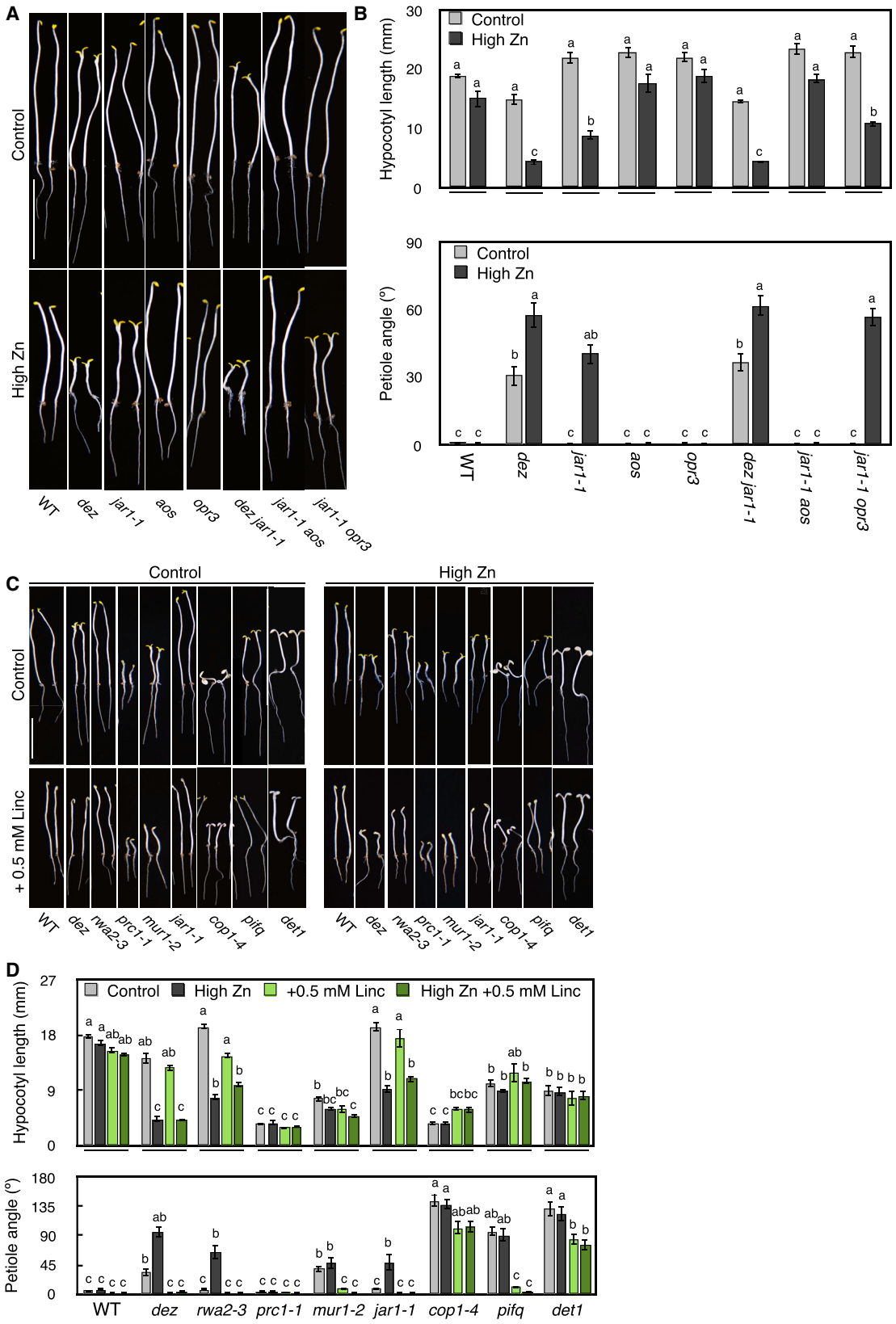

(legend on next page)

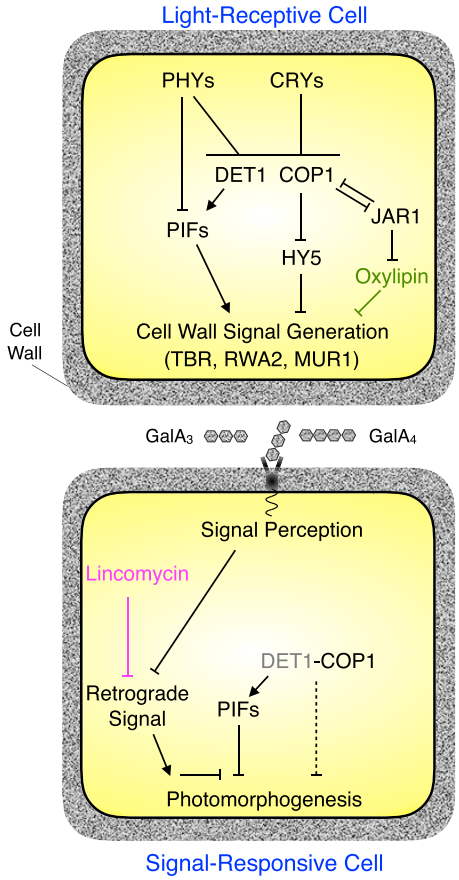

Figure 7. Integrated Model of the Control of Photomorphogenesis

Our data suggest that light perception is spatiotemporally separated from at least part of the photomorphogenic responses, different from previous models encompassing all of these events in a single cell. In continuous darkness, light-receptive cells generate a cell-wall-derived dark signal that acts on signal-responsive cells to repress photomorphogenesis. Disruption of specific pectin modifications in *dez* (*tbr*), *rwa2-3*, *mur1-2*, and *jar1* mutants interferes with the generation of the dark signal, resulting in constitutive photomorphogenesis. This phenotype can be rescued by addition of the vsOG tri- and tetra-galacturonate ($(GalA)_3$ and $(GalA)_4$), fragments of the pectin macromolecule homogalacturonan. Major players, *COP1* and *PIF*s, appear to act in both light-receptive and signal-responsive cells. *DET1*, *HY5*, and oxylipin signaling are important predominantly or only in light-receptive cells. A known retrograde signal acts in signal-responsive cells.

Taken together, our data indicate that TBR acts downstream of JAR1 in maintaining skotomorphogenesis.

Recent work has implicated a retrograde signal from plastids, which negatively interacts with PIFs, in the transcriptional control of PIF target genes. This was supported by the loss of cotyledon opening in the *pifq* mutant in the presence of lincomycin in the dark [53]. We confirmed the effect of lincomycin on *pifq*, and we additionally observed moderate partial effects on *cop1-4* and *det1* (Figures 6C and 6D). Similar to *pifq*, lincomycin suppressed cotyledon opening in *dez*, *rwa2-3*, *mur1-2*, and *jar1-1* in the dark. We detected only minor or no effects of lincomycin on hypocotyl length in *rwa2-3*, *jar1-1*, *pifq*, *dez*, and *mur1-2*, in agreement with published data on *pifq* [53].

DISCUSSION

An Extracellular Cell-Wall-Derived vsOG Dark Signal Controls Light-Dependent Development

Here, we show that mutants defective in the *TBR/DEZ* gene exhibit photomorphogenesis in the dark (Figures 1, 3, S1, and S3). Our data suggest an extracellular localization of the TBR/DEZ protein at tri-cellular junctions (Figures 4, 7, and S4), different from known regulators of light-dependent development [1]. *TBR/DEZ* expression is not light dependent at the transcript or protein level (http://bar.utoronto.ca/efp_arabidopsis/cgi-bin/efpWeb.cgi; Figure 4). We hypothesize that in wild-type *Arabidopsis* seedlings grown in darkness, photomorphogenic development is suppressed by an extracellularly generated dark signal, which is lacking in *dez* as a result of complex cell-wall defects (Figure 7). Accordingly, we were able to restore skotomorphogenic development in dark-grown *dez* seedlings through the supply of exogenous vsOG, very short, chemically unmodified fragments of the cell-wall pectin homogalacturonan, suggesting that $(GalA)_3$ and $(GalA)_4$ can act as a dark signal (Figures 5 and S5). When generated during cell-wall loosening in the process of hypocotyl elongation in the dark, for example, by endo-polygalacturonases or pectate lyases [13], vsOG could act in a feed-forward regulatory loop that suppresses photomorphogenesis. An extracellular dark signal provides a conceptual framework for the known irreversibility of photomorphogenesis, for example, through the controlled elimination of the vsOG signal upon the perception of light (e.g., similar to *jar1-1* and *jar1-11*, in which we propose the vsOG signal to be aberrantly eliminated in the dark; Figures 5 and 6; Table S3).

Known cell-wall-associated and cell-wall-derived signals depend predominantly on the status of pectin, one of three major types of cell-wall structural macromolecules [10, 14]. Among these signals, there is some evidence for roles of pectin fragments in cell-cell signaling. OGs (DP 10–15) are known to act as elicitors of defense responses against pathogen infection and in cell-wall integrity signaling during plant growth [13, 14]. Fewer studies reported effects of short OGs (DP 2–6), for example, in suppressing pathogen defense responses in wheat [54].

Figure 6. JA Biosynthesis Genes, *TBR*, and Retrograde Signaling in the Control of Photomorphogenesis

(A and B) Photographs (A) and quantification of morphological markers (B) of 7-day-old dark-grown wild-type (WT) and mutant seedlings cultivated on control (5 μM Zn) or high-Zn (100 μM Zn) media.

(C and D) Photographs (C) and quantification of morphological markers (D) of 7-day-old dark-grown wild-type and mutant seedlings cultivated on control or high-Zn media in the absence or presence of 0.5 mM lincomycin (Linc) to suppress plastid-derived retrograde signals.

Bar graphs indicate arithmetic means ± SD (n = 8 replicate seedlings); different letters denote statistically significant differences (Student's t test with Bonferroni corrections; $p < 0.05$). Scale bars, 10 mm.

See also Figure S6 and Table S2.

Localized light reception, followed by inter-organ and inter-cellular signaling, was invoked in the light-dependent control of seedling development based on a variety of previous experimental approaches, yet the molecular basis has remained unidentified [7, 34, 55, 56]. Thus, working models of the regulatory network controlling the switch from skotomorphogenic to photomorphogenic development have so far usually been depicted in a single cell. The results presented in this article strongly support the hypothesis that the cells receptive of the light stimulus are spatially or temporally ("spatiotemporally") separated from cells executing the repression or de-repression of photomorphogenesis (Figure 7).

Delineating a Pathway for Non-Cell-Autonomous Regulation of Light-Dependent Development

The cellulose synthase isoform PRC1 is required for enhanced hypocotyl elongation in the dark, but not for hypocotyl elongation in the light [42]. The *prc1-1* mutant was not photomorphogenic and not phenotypically rescued by exogenously applied vsOG (Figure 5). In addition, a *prc1-1 dez* double mutant was phenotypically *dez*-like, i.e., photomorphogenic (Table S3). Together, these observations are consistent with *PRC1* functioning in the growth process of hypocotyl elongation in the dark, with no signaling role. By contrast, *dez* exhibited multiple characteristics of photomorphogenic development (see Figure 1), including shortened hypocotyls and cotyledon opening in the dark, both of which were rescued by addition of vsOG. This indicates that vsOGs act to repress photomorphogenic development and are not merely rescuing a growth defect of *dez*. Other mutants identified here to exhibit *dez*-like phenotypes were also phenotypically complemented by the addition of vsOG. We envisage *RWA2* and *MUR1* functions to be necessary for the generation or the mobility of the extracellular vsOG signal, similar to *DEZ*. Differently, epistasis analysis suggested that, in dark-grown *jar1* mutants, both photomorphogenesis and its rescue by an additional mutation in the *AOS* gene occur upstream of *DEZ*, given that a *dez aos* double mutant was phenotypically *dez*-like (Figures 6 and S6).

Epistasis analysis, HY5 and PIF3 protein levels in dark-grown *dez*, and the responses of mutants to vsOG are consistent with roles of *PIF* and *COP1* genes in target cells responding to the extracellular dark signal, whereby only the function of *DET1* appears to predominate in light-receptive cells (Figures 2, 5, 7, and S5). Similar to the *pifq* mutant, the phenotypes of the *dez*, *rwa2*, *mur1*, and *jar1* mutants can be suppressed by lincomycin (Figure 6), which inhibits plastid translation and was proposed to eliminate a positive retrograde signal required for cotyledon opening [53]. This suggests that this retrograde signal acts in target cells responsive to the vsOG signal downstream of TBR/DEZ (Figure 7).

Interactions with the JA Pathway

We observed shortened hypocotyls and opened cotyledons in darkness in high-Zn-grown *jar1* mutants (Figure 5; Table S3). Somewhat contrastingly, *jar1* mutants were known for excessively elongated hypocotyls under low-intensity continuous far-red light, and JAR1 was reported to interact with the COP1 protein [57, 58]. In agreement with both observations, the rice *hebiba* mutant displays morphological characteristics of photomorphogenesis in the dark, as well as decreased responsiveness to far-red light. The *hebiba* mutant is defective in allene oxide cyclase, which acts in the plastid subsequent to AOS to catalyze the final step in the synthesis of the intermediates *cis*- and *dn*-OPDA in the JA biosynthesis pathway. Allene oxide, or one of its known degradation products, is a candidate molecule for triggering photomorphogenesis in dark-grown *hebiba* and *jar1* mutants. This molecule, however, is unlikely to act as the retrograde signal in target cells responsive to the vsOG signal, given that the addition of vsOG rescued the *jar1* mutant (see Figures 5 and 6).

Causality of Mutant Phenotypes

To ensure controlled and balanced supply of metal micronutrients, our laboratory uses media composed differently from those widespread in the plant community [26]. Thus, we observed photomorphogenesis in dark-grown *mur1* and *dez* mutants. Photomorphogenesis was enhanced under elevated Zn supply in the *dez* mutant and evident in in *rwa2-3* and *jar1* mutants in high-Zn conditions only (Figure 5; Table S3). The dose-dependent quantitative effect of Zn (Figure S1) was accompanied by marked increases in cell-wall thickness and in the degree of pectin methylesterification (Figures 4 and S4), suggesting that the *dez* mutation sensitized cell walls to Zn. The enhancement of photomorphogenesis in *dez* was metal specific to only Zn^{2+} and Ni^{2+} among a range of chemically similar divalent metal cations, reversed by an excess of chelator, and associated with Zn hypersensitivity in the light (Figures 1 and S1; Tables S1 and S2). The addition of vsOG separated the two phenotypes of *dez*, rescuing photomorphogenesis in the dark, but not Zn hypersensitivity in the light (Figures 5 and S5). We conclude that Zn hypersensitivity in the light is a second unrelated phenotype of the *dez* mutant, supported also by its absence in *rwa2-3* and in *jar1-1* mutants and by dark development of other Zn-hypersensitive mutants (Figures S1 and S5). We conclude that Zn is likely to act indirectly in enhancing photomorphogenesis in *dez*, *rwa2*, and *jar1* mutants, but we cannot fully exclude an alternative, more direct role of Zn^{2+} cations in photomorphogenesis that will require dedicated attention in the future. The proteins directly mediating the generation and perception of the cell wall signal remain to be identified, and we expect genetic redundancy or severe defects in loss-of-function mutants.

STAR★METHODS

Detailed methods are provided in the online version of this paper and include the following:

- KEY RESOURCES TABLE
- CONTACT FOR REAGENT AND RESOURCE SHARING
- EXPERIMENTAL MODEL AND SUBJECT DETAILS
- METHOD DETAILS
  - Plant Material and Growth Conditions
  - Biochemical Measurements
  - Immunoblots
  - Genetic Mapping
  - Transcriptomics

SUPPLEMENTAL INFORMATION

Supplemental Information includes six figures, five tables, and one data file and can be found with this article online at https://doi.org/10.1016/j.cub.2017.09.063.

AUTHOR CONTRIBUTIONS

Conceptualization, U.K., S.A.S., and M.J.H.; Methodology – Overall, S.A.S., M.J.H., and U.K.; Methodology – Specific, A.K., H.C.-M., D.G., and U.N.; Formal Analysis, S.A.S., M.J.H., U.K., L.B., C.L., H.C.-M., and R.J.S.; Investigation, S.A.S., M.J.H., L.B., C.L., and A.K.; Resources, S.A.S., U.K., M.J.H., D.B., U.N., D.G., H.C.M.; Data Curation, S.A.S., U.K., and M.J.H.; Writing – Original Draft, S.A.S. and U.K.; Writing – Reviewing and Editing, U.K., S.A.S., C.L., M.J.H., and A.K.; Visualization, S.A.S., U.K., C.L., H.C.-M., L.B., and R.J.S.; Supervision, U.K.; Project Administration, U.K. and S.A.S.; Funding Acquisition, U.K. and M.J.H.

ACKNOWLEDGMENTS

We thank Petra Düchting (Ruhr University Bochum, Germany) for multi-element analysis and the Paul Scherrer Institut (Villigen, Switzerland) and the European Synchrotron Radiation Source (ESRF, Grenoble, France) for beamtime at the microXAS beamline of the SLS and the ID21 beamlines, respectively. We thank Bradley Dotson and Chris Somerville (UC Berkeley) for sharing unpublished data, as well as Samantha Vernhettes and Herman Höfte (INRA Versailles, France), and Sascha Gille and Markus Pauly (UC Berkeley, CA), for sharing methods and for discussions. Funding was from the Deutsche Forschungsgemeinschaft (Kr1967/5-1 and 15-1; INST 213/803-1 FUGG), Ruhr University Bochum, and the European Union's Seventh Framework Program (FP7/2007-2013) under REA grant agreement nos. PIIF-GA-2008-219457 and PIEF-GA-2012-331680 (Marie Curie Actions) and CALIPSO (grant no. 312284).

Received: May 23, 2017
Revised: September 5, 2017
Accepted: September 28, 2017
Published: November 2, 2017

REFERENCES

1. Arsovski, A.A., Galstyan, A., Guseman, J.M., and Nemhauser, J.L. (2012). Photomorphogenesis. Arabidopsis Book *10*, e0147.
2. Von Arnim, A., and Deng, X.W. (1996). Light control of seedling development. Annu. Rev. Plant Physiol. Plant Mol. Biol. *47*, 215–243.
3. Huang, X., Ouyang, X., and Deng, X.W. (2014). Beyond repression of photomorphogenesis: role switching of COP/DET/FUS in light signaling. Curr. Opin. Plant Biol. *21*, 96–103.
4. Leivar, P., Monte, E., Oka, Y., Liu, T., Carle, C., Castillon, A., Huq, E., and Quail, P.H. (2008). Multiple phytochrome-interacting bHLH transcription factors repress premature seedling photomorphogenesis in darkness. Curr. Biol. *18*, 1815–1823.
5. Wang, Z.Y., Bai, M.Y., Oh, E., and Zhu, J.Y. (2012). Brassinosteroid signaling network and regulation of photomorphogenesis. Annu. Rev. Genet. *46*, 701–724.
6. Bou-Torrent, J., Roig-Villanova, I., and Martínez-García, J.F. (2008). Light signaling: back to space. Trends Plant Sci. *13*, 108–114.
7. Montgomery, B.L. (2016). Spatiotemporal phytochrome signaling during photomorphogenesis: From physiology to molecular mechanisms and back. Front. Plant Sci. *7*, 480.
8. Dong, J., Tang, D., Gao, Z., Yu, R., Li, K., He, H., Terzaghi, W., Deng, X.W., and Chen, H. (2014). Arabidopsis DE-ETIOLATED1 represses photomorphogenesis by positively regulating phytochrome-interacting factors in the dark. Plant Cell *26*, 3630–3645.
9. Gendreau, E., Traas, J., Desnos, T., Grandjean, O., Caboche, M., and Höfte, H. (1997). Cellular basis of hypocotyl growth in *Arabidopsis thaliana*. Plant Physiol. *114*, 295–305.
10. Wolf, S., Mouille, G., and Pelloux, J. (2009). Homogalacturonan methyl-esterification and plant development. Mol. Plant *2*, 851–860.
11. Cosgrove, D.J. (2016). Catalysts of plant cell wall loosening. F1000Res. *5*, 119.
12. Peaucelle, A., Wightman, R., and Höfte, H. (2015). The control of growth symmetry breaking in the *Arabidopsis* hypocotyl. Curr. Biol. *25*, 1746–1752.
13. Ferrari, S., Savatin, D.V., Sicilia, F., Gramegna, G., Cervone, F., and Lorenzo, G.D. (2013). Oligogalacturonides: plant damage-associated molecular patterns and regulators of growth and development. Front. Plant Sci. *4*, 49.
14. Wolf, S., Hématy, K., and Höfte, H. (2012). Growth control and cell wall signaling in plants. Annu. Rev. Plant Biol. *63*, 381–407.
15. Potikha, T., and Delmer, D.P. (1995). A mutant of *Arabidopsis thaliana* displaying altered patterns of cellulose deposition. Plant J. *7*, 453–460.
16. Gille, S., de Souza, A., Xiong, G., Benz, M., Cheng, K., Schultink, A., Reca, I.B., and Pauly, M. (2011). *O*-acetylation of *Arabidopsis* hemicellulose xyloglucan requires AXY4 or AXY4L, proteins with a TBL and DUF231 domain. Plant Cell *23*, 4041–4053.
17. Deng, X.-W., and Quail, P.H. (1992). Genetic and phenotypic characterization of *cop1* mutants of *Arabidopsis thaliana*. Plant J. *2*, 83–95.
18. Cabrera y Poch, H.L., Peto, C.A., and Chory, J. (1993). A mutation in the Arabidopsis *DET3* gene uncouples photoregulated leaf development from gene expression and chloroplast biogenesis. Plant J. *4*, 671–682.
19. Nisar, N., Li, L., Lu, S., Khin, N.C., and Pogson, B.J. (2015). Carotenoid metabolism in plants. Mol. Plant *8*, 68–82.
20. Chory, J., Nagpal, P., and Peto, C.A. (1991). Phenotypic and genetic analysis of *det2*, a new mutant that affects light-regulated seedling development in *Arabidopsis*. Plant Cell *3*, 445–459.
21. Chory, J., Peto, C., Feinbaum, R., Pratt, L., and Ausubel, F. (1989). *Arabidopsis thaliana* mutant that develops as a light-grown plant in the absence of light. Cell *58*, 991–999.
22. Deng, X.W., Caspar, T., and Quail, P.H. (1991). *cop*1: a regulatory locus involved in light-controlled development and gene expression in *Arabidopsis*. Genes Dev. *5*, 1172–1182.
23. Hou, Y., Von Arnim, A.G., and Deng, X.W. (1993). A new class of Arabidopsis constitutive photomorphogenic genes involved in regulating cotyledon development. Plant Cell *5*, 329–339.
24. Bischoff, V., Nita, S., Neumetzler, L., Schindelasch, D., Urbain, A., Eshed, R., Persson, S., Delmer, D., and Scheible, W.R. (2010). *TRICHOME BIREFRINGENCE* and its homolog *AT5G01360* encode plant-specific DUF231 proteins required for cellulose biosynthesis in Arabidopsis. Plant Physiol. *153*, 590–602.
25. Gille, S., and Pauly, M. (2012). *O*-acetylation of plant cell wall polysaccharides. Front. Plant Sci. *3*, 12.
26. Haydon, M.J., Kawachi, M., Wirtz, M., Hillmer, S., Hell, R., and Krämer, U. (2012). Vacuolar nicotianamine has critical and distinct roles under iron deficiency and for zinc sequestration in *Arabidopsis*. Plant Cell *24*, 724–737.
27. Weber, M., Deinlein, U., Fischer, S., Rogowski, M., Geimer, S., Tenhaken, R., and Clemens, S. (2013). A mutation in the *Arabidopsis thaliana* cell

wall biosynthesis gene *pectin methylesterase 3* as well as its aberrant expression cause hypersensitivity specifically to Zn. Plant J. *76*, 151–164.

28. Ang, L.H., and Deng, X.W. (1994). Regulatory hierarchy of photomorphogenic loci: allele-specific and light-dependent interaction between the *HY5* and *COP1* loci. Plant Cell *6*, 613–628.
29. Ang, L.-H., Chattopadhyay, S., Wei, N., Oyama, T., Okada, K., Batschauer, A., and Deng, X.-W. (1998). Molecular interaction between COP1 and HY5 defines a regulatory switch for light control of *Arabidopsis* development. Mol. Cell *1*, 213–222.
30. Oyama, T., Shimura, Y., and Okada, K. (1997). The *Arabidopsis HY5* gene encodes a bZIP protein that regulates stimulus-induced development of root and hypocotyl. Genes Dev. *11*, 2983–2995.
31. Kohchi, T., Mukougawa, K., Frankenberg, N., Masuda, M., Yokota, A., and Lagarias, J.C. (2001). The Arabidopsis *HY2* gene encodes phytochromobilin synthase, a ferredoxin-dependent biliverdin reductase. Plant Cell *13*, 425–436.
32. Koornneef, M., Rolff, E., and Spruit, C.J.P. (1980). Genetic control of light-inhibited hypocotyl elongation in *Arabidopsis thaliana* (L.) Heynh. Z. Pflanzenphysiol. *100*, 147–160.
33. Wolf, S., Mravec, J., Greiner, S., Mouille, G., and Höfte, H. (2012). Plant cell wall homeostasis is mediated by brassinosteroid feedback signaling. Curr. Biol. *22*, 1732–1737.
34. Kircher, S., and Schopfer, P. (2012). Photosynthetic sucrose acts as cotyledon-derived long-distance signal to control root growth during early seedling development in *Arabidopsis*. Proc. Natl. Acad. Sci. USA *109*, 11217–11221.
35. Dijkwel, P.P., Huijser, C., Weisbeek, P.J., Chua, N.H., and Smeekens, S.C. (1997). Sucrose control of phytochrome A signaling in Arabidopsis. Plant Cell *9*, 583–595.
36. Kurihara, Y., Makita, Y., Kawashima, M., Hamasaki, H., Yamamoto, Y.Y., and Matsui, M. (2014). Next-generation sequencing of genomic DNA fragments bound to a transcription factor *in vitro* reveals its regulatory potential. Genes (Basel) *5*, 1115–1131.
37. Nikolovski, N., Rubtsov, D., Segura, M.P., Miles, G.P., Stevens, T.J., Dunkley, T.P., Munro, S., Lilley, K.S., and Dupree, P. (2012). Putative glycosyltransferases and other plant Golgi apparatus proteins are revealed by LOPIT proteomics. Plant Physiol. *160*, 1037–1051.
38. Parsons, H.T., Christiansen, K., Knierim, B., Carroll, A., Ito, J., Batth, T.S., Smith-Moritz, A.M., Morrison, S., McInerney, P., Hadi, M.Z., et al. (2012). Isolation and proteomic characterization of the Arabidopsis Golgi defines functional and novel components involved in plant cell wall biosynthesis. Plant Physiol. *159*, 12–26.
39. de Souza, A., Hull, P.A., Gille, S., and Pauly, M. (2014). Identification and functional characterization of the distinct plant pectin esterases PAE8 and PAE9 and their deletion mutants. Planta *240*, 1123–1138.
40. Verhertbruggen, Y., Marcus, S.E., Haeger, A., Ordaz-Ortiz, J.J., and Knox, J.P. (2009). An extended set of monoclonal antibodies to pectic homogalacturonan. Carbohydr. Res. *344*, 1858–1862.
41. Tieman, D.M., and Handa, A.K. (1994). Reduction in pectin methylesterase activity modifies tissue integrity and cation levels in ripening tomato (*Lycopersicon esculentum* Mill.) fruits. Plant Physiol. *106*, 429–436.
42. Desnos, T., Orbović, V., Bellini, C., Kronenberger, J., Caboche, M., Traas, J., and Höfte, H. (1996). *Procuste1* mutants identify two distinct genetic pathways controlling hypocotyl cell elongation, respectively in dark- and light-grown *Arabidopsis* seedlings. Development *122*, 683–693.
43. Manabe, Y., Nafisi, M., Verhertbruggen, Y., Orfila, C., Gille, S., Rautengarten, C., Cherk, C., Marcus, S.E., Somerville, S., Pauly, M., et al. (2011). Loss-of-function mutation of *REDUCED WALL ACETYLATION2* in Arabidopsis leads to reduced cell wall acetylation and increased resistance to *Botrytis cinerea*. Plant Physiol. *155*, 1068–1078.
44. Manabe, Y., Verhertbruggen, Y., Gille, S., Harholt, J., Chong, S.L., Pawar, P.M., Mellerowicz, E.J., Tenkanen, M., Cheng, K., Pauly, M., and Scheller, H.V. (2013). Reduced Wall Acetylation proteins play vital and distinct roles in cell wall *O*-acetylation in Arabidopsis. Plant Physiol. *163*, 1107–1117.
45. Bonin, C.P., Potter, I., Vanzin, G.F., and Reiter, W.D. (1997). The *MUR1* gene of *Arabidopsis thaliana* encodes an isoform of GDP-D-mannose-4,6-dehydratase, catalyzing the first step in the de novo synthesis of GDP-L-fucose. Proc. Natl. Acad. Sci. USA *94*, 2085–2090.
46. Vanzin, G.F., Madson, M., Carpita, N.C., Raikhel, N.V., Keegstra, K., and Reiter, W.D. (2002). The *mur2* mutant of *Arabidopsis thaliana* lacks fucosylated xyloglucan because of a lesion in fucosyltransferase AtFUT1. Proc. Natl. Acad. Sci. USA *99*, 3340–3345.
47. Cescutti, P., and Rizzo, R. (2001). Divalent cation interactions with oligogalacturonides. J. Agric. Food Chem. *49*, 3262–3267.
48. Peña-Uribe, C.A., García-Pineda, E., Beltrán-Peña, E., and Reyes de la Cruz, H. (2012). Oligogalacturonides inhibit growth and induce changes in S6K phosphorylation in maize (*Zea mays* L. var. Chalqueño). Plant Growth Regul. *67*, 151–159.
49. Wasternack, C. (2007). Jasmonates: an update on biosynthesis, signal transduction and action in plant stress response, growth and development. Ann. Bot. *100*, 681–697.
50. Köster, J., Thurow, C., Kruse, K., Meier, A., Iven, T., Feussner, I., and Gatz, C. (2012). Xenobiotic- and jasmonic acid-inducible signal transduction pathways have become interdependent at the Arabidopsis *CYP81D11* promoter. Plant Physiol. *159*, 391–402.
51. Park, S.W., Li, W., Viehhauser, A., He, B., Kim, S., Nilsson, A.K., Andersson, M.X., Kittle, J.D., Ambavaram, M.M., Luan, S., et al. (2013). Cyclophilin 20-3 relays a 12-oxo-phytodienoic acid signal during stress responsive regulation of cellular redox homeostasis. Proc. Natl. Acad. Sci. USA *110*, 9559–9564.
52. Wasternack, C., and Hause, B. (2013). Jasmonates: biosynthesis, perception, signal transduction and action in plant stress response, growth and development. An update to the 2007 review in *Annals of Botany*. Ann. Bot. *111*, 1021–1058.
53. Martín, G., Leivar, P., Ludevid, D., Tepperman, J.M., Quail, P.H., and Monte, E. (2016). Phytochrome and retrograde signalling pathways converge to antagonistically regulate a light-induced transcriptional network. Nat. Commun. *7*, 11431.
54. Moerschbacher, B.M., Mierau, M., Graeßner, B., Noll, U., and Mor, A.J. (1999). Small oligomers of galacturonic acid are endogenous suppressors of disease resistance reactions in wheat leaves. J. Exp. Bot. *50*, 605–612.
55. Blum, D.E., Neff, M.M., and Van Volkenburgh, E. (1994). Light-stimulated cotyledon expansion in the *blu3* and *hy4* mutants of *Arabidopsis thaliana*. Plant Physiol. *105*, 1433–1436.
56. Ranjan, A., Fiene, G., Fackendahl, P., and Hoecker, U. (2011). The *Arabidopsis* repressor of light signaling SPA1 acts in the phloem to regulate seedling de-etiolation, leaf expansion and flowering time. Development *138*, 1851–1862.
57. Chen, I.C., Huang, I.C., Liu, M.J., Wang, Z.G., Chung, S.S., and Hsieh, H.L. (2007). Glutathione *S*-transferase interacting with far-red insensitive 219 is involved in phytochrome A-mediated signaling in Arabidopsis. Plant Physiol. *143*, 1189–1202.
58. Wang, J.G., Chen, C.H., Chien, C.T., and Hsieh, H.L. (2011). FAR-RED INSENSITIVE219 modulates CONSTITUTIVE PHOTOMORPHOGENIC1 activity via physical interaction to regulate hypocotyl elongation in Arabidopsis. Plant Physiol. *156*, 631–646.
59. Bernal, M., Casero, D., Singh, V., Wilson, G.T., Grande, A., Yang, H., Dodani, S.C., Pellegrini, M., Huijser, P., Connolly, E.L., et al. (2012). Transcriptome sequencing identifies *SPL7*-regulated copper acquisition genes *FRO4*/*FRO5* and the copper dependence of iron homeostasis in *Arabidopsis*. Plant Cell *24*, 738–761.

60. Curtis, M.D., and Grossniklaus, U. (2003). A gateway cloning vector set for high-throughput functional analysis of genes in planta. Plant Physiol. *133*, 462–469.

61. Clough, S.J., and Bent, A.F. (1998). Floral dip: a simplified method for *Agrobacterium*-mediated transformation of *Arabidopsis thaliana*. Plant J. *16*, 735–743.

62. Nakata, M., Mitsuda, N., Herde, M., Koo, A.J., Moreno, J.E., Suzuki, K., Howe, G.A., and Ohme-Takagi, M. (2013). A bHLH-type transcription factor, ABA-INDUCIBLE BHLH-TYPE TRANSCRIPTION FACTOR/JA-ASSOCIATED MYC2-LIKE1, acts as a repressor to negatively regulate jasmonate signaling in *Arabidopsis*. Plant Cell *25*, 1641–1656.

63. Porra, R.J., Thompson, W.A., and Kreidemann, P.E. (1989). Determination of accurate extinction coefficients and simultaneous equations for assaying chlorophylls *a* and *b* extracted with four different solvents: verification of the concentration of chlorophyll standards by atomic absorption spectroscopy. Biochim. Biophys. Acta. *975*, 384–394.

64. Wellburn, A.R. (1994). The spectral determination of chlorophylls *a* and *b*, as well as total carotenoids, using various solvents with spectrophotometers of different resolution. J. Plant Physiol. *144*, 307–313.

65. Günl, M., Kraemer, F., and Pauly, M. (2011). Oligosaccharide mass profiling (OLIMP) of cell wall polysaccharides by MALDI-TOF/MS. In The Plant Cell Wall: Methods and Protocols, *Volume 715*, Z.A. Popper, ed. (Springer Science+Business Media), pp. 43–54.

66. Müller, K., Levesque-Tremblay, G., Bartels, S., Weitbrecht, K., Wormit, A., Usadel, B., Haughn, G., and Kermode, A.R. (2013). Demethylesterification of cell wall pectins in Arabidopsis plays a role in seed germination. Plant Physiol. *161*, 305–316.

67. Cesaretti, M. (2003). A 96-well assay for uronic acid carbazole reaction. Carbohydr. Polym. *54*, 59–61.

68. Galvão, R.M., Li, M., Kothadia, S.M., Haskel, J.D., Decker, P.V., Van Buskirk, E.K., and Chen, M. (2012). Photoactivated phytochromes interact with HEMERA and promote its accumulation to establish photomorphogenesis in *Arabidopsis*. Genes Dev. *26*, 1851–1863.

69. Chai, T., Zhou, J., Liu, J., and Xing, D. (2015). LSD1 and HY5 antagonistically regulate red light induced-programmed cell death in *Arabidopsis*. Front. Plant Sci. *6*, 292.

70. Du, Z., Zhou, X., Ling, Y., Zhang, Z., and Su, Z. (2010). agriGO: a GO analysis toolkit for the agricultural community. Nucleic Acids Res. *38*, W64–W70.

71. Martin, F.L., Kelly, J.G., Llabjani, V., Martin-Hirsch, P.L., Patel, I.I., Trevisan, J., Fullwood, N.J., and Walsh, M.J. (2010). Distinguishing cell types or populations based on the computational analysis of their infrared spectra. Nat. Protoc. *5*, 1748–1760.

72. Wehrens, R. (2011). Chemometrics with R: Multivariate Data Analysis in the Natural Sciences and Life Sciences (Springer).

73. R Development Core Team (2015). R: A language and environment for statistical computing (R Foundation for Statistical Computing). https://www.r-project.org/.

74. Kuhn, M. (2016). Caret: classification and regression training (R Foundation for Statistical Computing). https://github.com/topepo/caret/.

75. R-Forge (2013). Signal: signal processing (R Foundation for Statistical Computing). http://r-forge.r-project.org/projects/signal/.

76. Sarret, G., Willems, G., Isaure, M.P., Marcus, M.A., Fakra, S.C., Frérot, H., Pairis, S., Geoffroy, N., Manceau, A., and Saumitou-Laprade, P. (2009). Zinc distribution and speciation in *Arabidopsis halleri* × *Arabidopsis lyrata* progenies presenting various zinc accumulation capacities. New Phytol. *184*, 581–595.

77. Ravel, B., and Newville, M. (2005). ATHENA, ARTEMIS, HEPHAESTUS: data analysis for X-ray absorption spectroscopy using IFEFFIT. J. Synchrotron Radiat. *12*, 537–541.

78. Micali, C.O., Neumann, U., Grunewald, D., Panstruga, R., and O'Connell, R. (2011). Biogenesis of a specialized plant-fungal interface during host cell internalization of *Golovinomyces orontii* haustoria. Cell. Microbiol. *13*, 210–226.

79. Haydon, M.J., and Cobbett, C.S. (2007). A novel major facilitator superfamily protein at the tonoplast influences zinc tolerance and accumulation in Arabidopsis. Plant Physiol. *143*, 1705–1719.

80. Noguchi, T., Fujioka, S., Takatsuto, S., Sakurai, A., Yoshida, S., Li, J., and Chory, J. (1999). Arabidopsis *det2* is defective in the conversion of (24R)-24-methylcholest-4-En-3-one to (24R)-24-methyl-5alpha-cholestan-3-one in brassinosteroid biosynthesis. Plant Physiol. *120*, 833–840.

81. Wang, Z.Y., Nakano, T., Gendron, J., He, J., Chen, M., Vafeados, D., Yang, Y., Fujioka, S., Yoshida, S., Asami, T., and Chory, J. (2002). Nuclear-localized BZR1 mediates brassinosteroid-induced growth and feedback suppression of brassinosteroid biosynthesis. Dev. Cell *2*, 505–513.

82. Hématy, K., Sado, P.E., Van Tuinen, A., Rochange, S., Desnos, T., Balzergue, S., Pelletier, S., Renou, J.P., and Höfte, H. (2007). A receptor-like kinase mediates the response of *Arabidopsis* cells to the inhibition of cellulose synthesis. Curr. Biol. *17*, 922–931.

83. Reiter, W.D., Chapple, C.C., and Somerville, C.R. (1993). Altered growth and cell walls in a fucose-deficient mutant of *Arabidopsis*. Science *261*, 1032–1035.

84. Staswick, P.E., Tiryaki, I., and Rowe, M.L. (2002). Jasmonate response locus *JAR1* and several related Arabidopsis genes encode enzymes of the firefly luciferase superfamily that show activity on jasmonic, salicylic, and indole-3-acetic acids in an assay for adenylation. Plant Cell *14*, 1405–1415.

85. Ellis, C., and Turner, J.G. (2002). A conditionally fertile *coi1* allele indicates cross-talk between plant hormone signalling pathways in *Arabidopsis thaliana* seeds and young seedlings. Planta *215*, 549–556.

86. Park, J.H., Halitschke, R., Kim, H.B., Baldwin, I.T., Feldmann, K.A., and Feyereisen, R. (2002). A knock-out mutation in allene oxide synthase results in male sterility and defective wound signal transduction in *Arabidopsis* due to a block in jasmonic acid biosynthesis. Plant J. *31*, 1–12.

87. Stintzi, A., and Browse, J. (2000). The *Arabidopsis* male-sterile mutant, *opr3*, lacks the 12-oxophytodienoic acid reductase required for jasmonate synthesis. Proc. Natl. Acad. Sci. USA *97*, 10625–10630.

88. Lincoln, C., Britton, J.H., and Estelle, M. (1990). Growth and development of the *axr1* mutants of *Arabidopsis*. Plant Cell *2*, 1071–1080.

89. Chao, Q., Rothenberg, M., Solano, R., Roman, G., Terzaghi, W., and Ecker, J.R. (1997). Activation of the ethylene gas response pathway in Arabidopsis by the nuclear protein ETHYLENE-INSENSITIVE3 and related proteins. Cell *89*, 1133–1144.

90. Vandenbussche, F., Habricot, Y., Condiff, A.S., Maldiney, R., Van der Straeten, D., and Ahmad, M. (2007). HY5 is a point of convergence between cryptochrome and cytokinin signalling pathways in *Arabidopsis thaliana*. Plant J. *49*, 428–441.

91. Sung, D.Y., Lee, D., Harris, H., Raab, A., Feldmann, J., Meharg, A., Kumabe, B., Komives, E.A., and Schroeder, J.I. (2007). Identification of an arsenic tolerant double mutant with a thiol-mediated component and increased arsenic tolerance in *phyA* mutants. Plant J. *49*, 1064–1075.

92. Vogel, J.P., Schuerman, P., Woeste, K., Brandstatter, I., and Kieber, J.J. (1998). Isolation and characterization of Arabidopsis mutants defective in the induction of ethylene biosynthesis by cytokinin. Genetics *149*, 417–427.

93. Moore, B., Zhou, L., Rolland, F., Hall, Q., Cheng, W.H., Liu, Y.X., Hwang, I., Jones, T., and Sheen, J. (2003). Role of the *Arabidopsis* glucose sensor HXK1 in nutrient, light, and hormonal signaling. Science *300*, 332–336.

94. Scheible, W.R., Eshed, R., Richmond, T., Delmer, D., and Somerville, C. (2001). Modifications of cellulose synthase confer resistance to isoxaben and thiazolidinone herbicides in *Arabidopsis ixr1* mutants. Proc. Natl. Acad. Sci. USA *98*, 10079–10084.

95. Finkelstein, R.R., and Lynch, T.J. (2000). The Arabidopsis abscisic acid response gene *ABI5* encodes a basic leucine zipper transcription factor. Plant Cell *12*, 599–609.

96. Koornneef, M., Reuling, G., and Karssen, C.M. (1984). The isolation and characterization of abscisic acid-insensitive mutants of *Arabidopsis thaliana*. Physiol. Plant. *61*, 377–383.

97. Guzmán, P., and Ecker, J.R. (1990). Exploiting the triple response of *Arabidopsis* to identify ethylene-related mutants. Plant Cell *2*, 513–523.

98. Reiter, W.D., Chapple, C., and Somerville, C.R. (1997). Mutants of *Arabidopsis thaliana* with altered cell wall polysaccharide composition. Plant J. *12*, 335–345.

99. Peng, L., Hocart, C.H., Redmond, J.W., and Williamson, R.E. (2000). Fractionation of carbohydrates in *Arabidopsis* root cell walls shows that three radial swelling loci are specifically involved in cellulose production. Planta *211*, 406–414.

100. Desprez, T., Juraniec, M., Crowell, E.F., Jouy, H., Pochylova, Z., Parcy, F., Höfte, H., Gonneau, M., and Vernhettes, S. (2007). Organization of cellulose synthase complexes involved in primary cell wall synthesis in *Arabidopsis thaliana*. Proc. Natl. Acad. Sci. USA *104*, 15572–15577.

STAR★METHODS

KEY RESOURCES TABLE

REAGENT or RESOURCE	SOURCE	IDENTIFIER
Antibodies		
LM19	Plant Probes	Cat#LM19
LM20	Plant Probes	Cat#LM20
Goat Anti-Rat IgG H&L (10 nm Gold)	PLANO GmbH	Cat#EM.GAT10
Anti-HY5	Agrisera	Cat#AS12 1867
Anti-PIF3	Agrisera	Cat#AS16 3954
Anti-Actin	Agrisera	Cat#AS13 2640
Goat Anti-Rabbit IgG, HRP conjugate	Agrisera	Cat#AS09 602
Rabbit Anti-Goat IgG, HRP conjugate	Agrisera	Cat#AS09 605
Bacterial and Virus Strains		
E. coli DH5α	N/A	N/A
A. tumefaciens GV3031	N/A	N/A
Chemicals, Peptides, and Recombinant Proteins		
Protease Cocktail inhibitor	abmGood	Cat#G135
Ethylene glycol-bis(2-aminoethylether)-N,N,N′,N′-tetraacetic acid (EGTA) ≥ 97%	Sigma	Cat#E3889
1,2-Diaminocyclohexanetetraacetic acid monohydrate (CDTA) ≥ 98.5%	Sigma	Cat#D1383
Ethylenediaminetetraacetic acid (EDTA) ≥ 99%	Sigma	Cat#EDS
1-Naphthaleneacetic acid (NAA) ≥ 95%	Sigma	Cat#N0640
N-(1-Naphthyl)phthalamidic acid (NPA) ≥ 95%	Sigma	Cat#33371
1-Naphthoxyacetic acid (NOA) ≥ 98%	Sigma	Cat#255416
Gibberellic Acid (GA3) 90-100%	Sigma	Cat#36575
α-tert-Butyl-β-(4-chlorobenzyl)-1H-1,2,4-triazole-1-ethanol (Paclobutrazol) ≥ 98%	Sigma	Cat#46046
Epibrassinolide (EBL) ≥ 85%	Sigma	Cat#E1641
Brassinazole (BRZ) ≥ 98%	Sigma	Cat#SML1406
1-aminocyclopropane-1-carboxylic acid (ACC) ≥ 98%	Sigma	Cat#736260
Aminoethoxyvinyl glycine hydrochloride (AVG) ≥ 98%	Sigma	Cat#32999
Methyl Jasmonate (MeJA) ≥ 95%	Sigma	Cat#392707
Cyclopropanecarboxylic acid (Coronatine) ≥ 95%	Sigma	Cat#C8115
(±)-Abscisic acid (ABA) ≥ 98.5%	Sigma	Cat#A1049
Thidiazuron ≥ 98%	Sigma	Cat#45686
4-Chloro-5-(methylamino)-2-(α,α,α-trifluoro-m-tolyl)-3(2H)-pyridazinone (Norflurazon) ≥ 98%	Sigma	Cat#34364
Lincomycin ≥ 95%	Sigma	Cat#62143
Diphenyleneiodonium chloride (DPI) ≥ 98%	Sigma	Cat#D2926
Isoxaben ≥ 98%	Santa Cruz Biotechnology	Cat#sc-235431
α-Cyclopropyl-α-(4-methoxyphenyl)-5-pyrimidinemethanol (Ancymidol) ≥ 98%	Sigma	Cat#A9431
(−)-Epigallocatechin gallate (EGCG) ≥ 97%	Sigma	Cat#50299
Methyl viologen dichloride hydrate (Paraquat) ≥ 98%	Sigma	Cat#856177
Di-galacturonic acid (2-GalA) ≥ 85%	Sigma	Cat#D4288
Tri-galacturonic acid (3-GalA) ≥ 95%	Sigma	Cat#T7407
Tetra-galacturonic acid (4-GalA) ≥ 95%	Santa Cruz Biotechnology	Cat#sc-474867

(*Continued on next page*)

Continued

REAGENT or RESOURCE	SOURCE	IDENTIFIER
Polygalacturonic acid (PGA) ≥ 95%	Sigma	Cat#81325
TRIS ≥ 95%	Sigma	Cat#1503
NaCl	Sigma	Cat#S7653
Glycerol	Sigma	Cat#G5516
DL-1,4-Dithiothreitol (DTT)	Boehringer	Cat#AC327190500
β-Mercaptoethanol	Roth	Cat#4227.1
Phenylmethylsulfonyl fluoride (PMSF)	Sigma	Cat#78830
N-ethylmaleimide	Sigma	Cat#E3876
MG-115	Sigma	Cat#SCP0005
MG-132	Sigma	Cat#474787
cOmplete EDTA-free Protease Inhibitor Cocktail	Sigma	Cat#COEDTAF-RO
Phosphatase Inhibitor Cocktail 3	Sigma	Cat#P0044
Polyvinyl polypyrrolidone	Sigma	Cat#77627
Polyvinylpyrrolidone (PVP-40)	Sigma	Cat#PVP40
Sodium Dodecyl Sulfate (SDS)	AppliChem	Cat#A2263
Critical Commercial Assays		
Acetic Acid Assay	Megazyme, Bray	Cat#K-ACET
TRIzol Reagent	Thermofisher Scientific	Cat#15596026
LR Clonase II Plus	Thermofisher Scientific	Cat#12538200
Pectin Methylesterase Assay	[66]	N/A
Pectin Methylesterase from orange peel	Sigma	Cat#P5400
Alcohol oxidase	Sigma	Cat#A2404
Formaldehyde dehydrogenase	Sigma	Cat#F1879
Formaldehyde dehydrogenase	Sigma	Cat#F1879
Endopolygalacturonase	Megazyme	Cat#EC3.2.1.15
Genome ATH1 Array	Affymetrix	Cat#900385
RNA Plant Mini-Kit	QIAGEN	Cat#74903
SuperScript III	Invitrogen	Cat#18080093
SYBR Green PCR Master Mix	Applied Biosystems	Cat#4309155
Phusion High Fidelity DNA Polymerase	Thermofisher Scientific	Cat#F530S
DNA-free DNA removal Kit	Ambion	Cat#AM1906
Pectolyase Y-23	Duchefa	Cat#P8004
LightCycler 480 High Resolution Melting Master	Roche Life Sciences	Cat#04909631001
ECL Select	GE Healthcare	Cat#RPN2235
LightCycler 480 High Resolution Melting Master	Roche Life Sciences	Cat#04909631001
Deposited Data		
Microarray data	This paper	GEO: GSE96589
Experimental Models: Organisms/Strains		
Landsberg *erecta*	NASC	NASC ID: NW20
Col-0	NASC	NASC ID: 70000
ZIF1prom::GUS	[79]	N/A
tbr-1	[15]	N/A
det3	[18]	N/A
cop1-4	[17]	N/A
ozs1	[27]	N/A
ozs2	[27]	N/A
zif1	[79]	N/A
det1	[21]	N/A

(*Continued on next page*)

Continued

REAGENT or RESOURCE	SOURCE	IDENTIFIER
pifq	[4]	N/A
hy5-215	[30]	N/A
hy2 (WiscDsLoxHs147_05H)	NASC	NASC ID: N914056
bri1-5	[80]	N/A
bzr1-1D	[81]	N/A
rwa2-3	[43]	N/A
prc1-1	[82]	N/A
mur1-2	[83]	N/A
jar1-1	[84]	N/A
jar1-11	[84]	N/A
coi1-16	[85]	N/A
aos	[86]	N/A
jar1-1 aos	[50]	N/A
opr3	[87]	N/A
axr1-3	[88]	N/A
ein3	[89]	N/A
esk1-2 (SALK_078275C)	NASC	NASC ID: N2107292
axy4-2 (SALK_120594C)	NASC	NASC ID: N663833
cry1 2	[90]	N/A
phya-t (SALK_014575)	[91]	N/A
gun1 (SALK_096816C)	NASC	NASC ID: N676301
rwa1 (SAIL_205_F09)	NASC	NASC ID: N872102
rwa3 (SAIL_776_A08)	NASC	NASC ID: N834704
rwa4 (SALK_142291C)	NASC	NASC ID: N677199
cin4-1	[92]	N/A
det1-1	[21]	N/A
hxk1-1 (gin2-1)	[93]	N/A
qrt1 (SAIL_140_C11)	NASC	NASC ID: N873242
det2-1	[20]	N/A
ixr1-2	[94]	N/A
abi5-1	[95]	N/A
abi3-1	[96]	N/A
fer-4 (GK_106_A06)	NASC	NASC ID: N69044
the1-1	[82]	N/A
qua1 (SALK_004353C)	NASC	NASC ID: N660685
eto1-1	[97]	N/A
csu1 (SALK_060493C)	NASC	NASC ID: N686069
xxt1 xxt2 (SAIL_785_E02, SALK_101308)	NASC	NASC ID: N16349
tbl1-3 (SALK_135222C)	NASC	NASC ID: N680315
mur2-1	[98]	N/A
prc1-1	[42]	N/A
rsw1-1	[99]	N/A
rsw2-1	[99]	N/A
ixr2-1	[100]	N/A
wak1 (SALK_107175)	NASC	NASC ID: N607175
spa1 2 3	[56]	N/A
Oligonucleotides		
See Table S5	N/A	N/A

(*Continued on next page*)

Continued		
REAGENT or RESOURCE	SOURCE	IDENTIFIER
Recombinant DNA		
pENTR D-TOPO	Thermofisher Scientific	Cat#K240020
pMDC107	[60]	N/A
pMDC107; genomic TBR	This paper	N/A
Software and Algorithms		
Parametric Analysis of Gene Set Enrichment (PAGE)	[70]	N/A
GeneSpring GX 7	Agilent	N/A
OMNIC	Thermofisher Scientific	N/A
R statistical software	[73]	N/A
R statistical software - caret package	[74]	N/A
R statistical software - signal package	[75]	N/A
Excel	Microsoft	N/A
Access	Microsoft	N/A
Athena	[77]	N/A
Light Cycler Software	Roche Life Sciences	RRID: SCR_012155

CONTACT FOR REAGENT AND RESOURCE SHARING

Further information and requests for resources and reagents should be directed to and will be fulfilled by the Lead Contact, Ute Krämer (ute.kraemer@ruhr-uni-bochum.de).

EXPERIMENTAL MODEL AND SUBJECT DETAILS

The *Arabidopsis thaliana* (L.) accession Columbia (Col-0) and Landsberg erecta (Ler), as well as mutants were obtained from the Nottingham *Arabidopsis* Stock Centre (NASC; Key Resources Table). For more information see http://www.arabidopsis.org/portals/education/aboutarabidopsis.jsp.

METHOD DETAILS

Plant Material and Growth Conditions

Arabidopsis thaliana Col-0 wild-type or mutant seeds were surface sterilized using chlorine gas for 3 to 4 hr and sown on modified Hoagland's medium [59] containing 1% (w/v) sucrose and solidified with 0.8% (w/v) Agar Type M (Sigma, Steinheim, Germany) in ambient daylight, followed by stratification in the dark at 4°C for 2 d. Seedlings were cultivated on vertically-orientated square (120 mm x 120 mm) polypropylene petri dishes in a 16 hr day (120 μmol m^{-2} s^{-1}, 22°C), 8 hr night (18°C) cycle in a growth chamber (Percival CU-41L4, CLF Climatics, Emersacker, Germany) for 7 d. For cultivation in darkness, seedlings were left in ambient daylight for 2 to 3 hr after sowing, then wrapped in 2 layers of aluminum foil and placed next to light-grown seedlings. Control media contained 1 or 5 μM Zn as indicated, and high-Zn media contained 100 μM Zn. Hypocotyl length, petiole angle and root length were quantified using ImageJ software (http://imagej.nih.gov/ij/), after scanning on a flatbed scanner. All supplements, including additional metals, chelators, hormones, hormone inhibitors or other chemicals, were added after sterile filtration (syringe and single-use filter MILLEX-GV 0.22 μm, Millipore, Bedford, MA, USA) in the concentrations indicated to autoclaved control media, generating an additional control containing the same volume of solvent if applicable. To generate double mutants, crosses were performed, and double mutants selected on the basis of phenotype, with the exception of *tbl1-3, cry1, cry2* and *wak1* that were genotyped by PCR or sequencing. For harvesting dark-grown seedlings, the double aluminum foil cover was removed from plates in dim green light and seedlings were flash frozen and homogenized with a mortar and pestle in liquid nitrogen.

The mutant lines used in this study are listed in the Key Resources Table. To generate the *TBR* genomic construct (*TBRgenomic::GFP*) for complementation of the *dez* mutant, a DNA fragment of 4,083 bp in size (beginning 1,615 bp upstream of the translational start codon and ending one codon before the translational stop codon) was obtained by PCR using wild-type genomic DNA as a template, cloned into the Gateway pENTR vector (Invitrogen, Carlsbad, USA), and subsequently transferred into pMDC107 [60] containing a 3′ cDNA encoding EFGP using LR Clonase II (Invitrogen, Carlsbad, USA). This was transformed into the *Agrobacterium tumefaciens* strain GV3031, and *A. thaliana* (*dez*) were transformed using the floral dip method [61].

Biochemical Measurements

Anthocyanin contents of seedlings were determined according to a published protocol [62]. Homogenized tissue was incubated in methanol at room temperature (RT) for 5 min, centrifuged at 14,000 rpm at RT for 5 min, and the absorbance of the supernatant determined at 530 and 657 nm to correct for chlorophyll (Total anthocyanin [g^{-1} FW] = A_{530} - (0.25 x A_{657})). Photosynthetic pigment contents were determined upon extracting pigments from homogenized tissue in methanol at room temperature (chlorophyll [$\mu g\ mL^{-1}$] = 22.5 · A_{650} + 4.0 · A_{665}; carotene [$\mu g\ mL^{-1}$] = (1,000 · A_{470} - 2.860 · (15.65 · A_{666} - 7.340 · A_{653}) - 129.2 · ((27.05 · A_{653} - 11.21 · A_{666}) / 245)) [63, 64].

To quantify pectin modifications, Alcohol Insoluble Residue (AIR) was prepared from seedlings snap-frozen in 2-mL polypropylene tubes in liquid N_2, freeze-dried, and homogenized in a mortar using a pestle [65]. One mL of 70% (v/v) ethanol was added to each sample, vortexed and centrifuged at 20,000x*g* for 20 min. The supernatant was discarded, and the procedure repeated with 1 mL of a 1:1 mixture of methanol and chloroform. After discarding the supernatant, the AIR pellet was air-dried. To isolate pectin from AIR for measuring methylesterification, AIR was incubated at 95°C for 15 min in an extraction buffer containing 50 mM 1,2-Diaminocyclohexanetetraacetic acid (CDTA) and 50 mM TRIS (pH 7.2). Samples were then centrifuged at 10,000x*g* for 10 min, and the supernatant contained the pectin. To determine methylesterification of the extracted pectin, an enzymatic assay was performed as described [66]. Pectin methylesterase activity was determined using the same assay, using 20 μg total protein extracted from seedlings and 100 μg of pectin (apple pectin; Sigma, Steinheim, Germany), at pH 7.5. Use of CDTA interferes with the measurement of pectin acetylation. Thus pectin acetylation was quantified after digesting AIR with 2 mU mL^{-1} endo-polygalacturonases (EC3.2.1.15; Megazyme, Wicklow, Ireland) and 0.04 mU mL^{-1} pectin methylesterase (PME; Sigma, Steinheim, Germany) in 50 mM ammonium formate containing 2 $\mu g\ mL^{-1}$ sodium azide, pH 4.5, at 37°C for 17 hr. This reaction was inactivated by incubating at 80°C for 20 min, then centrifuged at 3,220 x *g* for 15 min. The supernatant was freeze-dried, then 150 μL of 1 M NaOH was added to each tube. Tubes were incubated at room temperature for 90 min with shaking at 600 rpm, then neutralized with 150 μL of 1 M HCl. Acetic acid was quantified in this solution using the Megazyme kit and protocol (K-ACET, Megazyme, Wicklow, Ireland).

In each pectin extract or digest, uronic acid was quantified using known concentrations of galacturonic acid as a standard [67]. Briefly, 50 μL of pectin solution was incubated with 200 μL 25 mM sodium tetraborate in 10 M H_2SO_4 for 10 min at 100°C, allowed to cool, then 50 μL 0.125% (w/v) carbazole in 100% (v/v) ethanol added to each reaction and again incubated for 10 min at 100°C. After cooling, absorbances were read at 550 nm.

Immunoblots

Seven-d-old seedlings were harvested from agar-solidified control and high-Zn media in dim green light for dark-grown and in ambient light for light-grown seedlings. For PIF3 detection [68], 80 seedlings were harvested directly into 500 μL extraction buffer (100 mM TRIS-HCl pH 7.5, 100 mM NaCl, 5% (w/v) SDS, 5 mM EDTA, 20% (v/v) glycerol, 20 mM DTT, 40 mM β-mercaptoethanol, 2 mM phenylmethylsulfonyl fluoride (PMSF), 10 mM N-ethylmaleimide, 80 μM MG132, 80 μM MG115, 1 × EDTA-free protease inhibitor cocktail, 1 × phosphatase inhibitor cocktail 3) and ground using a micro-pestle. For HY5 detection [69], seedlings were harvested and ground to powder in liquid nitrogen and 50 mM TRIS–HCl (pH 6.8), 50 mM DTT, 4% (w/v) SDS, 10% (v/v) glycerol, 1% (w/v) polyvinylpolypyrrolidone (PVPP), 5 mM PMSF. After vortexing and centrifugation at 14,000 rpm for 15 min, protein concentration was determined in the supernatant using the Pierce BCA Protein Assay Kit (ThermoScientific, Rockford, USA). For HY5 immunoblots, 45 μg protein was loaded onto an 8% (w/v) SDS-PAGE gel, and for PIF3, 20 μL of fresh protein extract were loaded onto a 15% (w/v) SDS-PAGE gel. Gels were run at 200 V at RT for 1.5 hr, followed by wet/tank transfer to PVDF membranes (4°C, 30V, overnight). After blocking with 5% (w/v) milk powder and 1% (w/v) polyvinylpyrrolidone (PVP-40) in TRIS-buffered saline containing 0.1% (v/v) Tween-20 (TBST) for 1 hr, membranes were incubated with the primary antibody (anti-HY5, anti-PIF3 or anti-Actin; Agrisera, Vännas, Sweden) diluted 1:500 (1:5,000 for anti-Actin) in TBST containing 1% (w/v) milk powder at 4°C overnight (TBSTM). Membranes were washed in TBSTM for 1 hr, then incubated with an HRP-conjugated secondary antibody (Agrisera, Vännas, Sweden) diluted 1:10,000 in TBSTM. After a brief wash in TBSTM, detection was carried out with ECL Select HRP substrate (GE Healthcare, Little Chalfont, England) using a Fusion Fx7 GelDoc (Vilber Lourmat, Eberhardzell, Germany).

Genetic Mapping

After backcrossing, homozygous F3 plants with the *dez* phenotype were crossed to Ler-0 to generate F2 mapping populations with the *dez* phenotype segregating 3:1 (181 wild-type: 65 *dez*, X^2 = 0.27, p = 0.6). Seven pools of five *dez* seedlings each were used in Bulk Segregant Analysis mapping using 25 Cleaved Amplified Polymorphic Sites (CAPS) and Single Sequence Length Polymorphism (SSLP) markers distributed across the genome isolate the *dez* mutation to an area close to CIW17 and ASA1 on chromosome 5. Fine scale mapping, using a combination of CAPS, SSLP and SNP genotyping using High Resolution Melt (HRM) analysis of 550 F2 individuals located the genetic lesion responsible for the *dez* phenotype between PERL0870687 and SNP13752, a region containing 21 genes. After extracting genomic DNA from *dez* plants genes in this region were PCR amplified and sequenced, and the polymorphism responsible for *dez* identified in the *TBR* gene.

Transcriptomics

Total RNA was extracted from ~45 7-day-old dark-grown seedlings using an RNeasy Plant RNA Kit (QIAGEN, Hilden, Germany). Labeling and hybridization to ATH1 microarray chips (Affymetrix, High Wycombe, UK) was performed by the EMBL Genomics Core Facility (Heidelberg, Germany). Data analysis was performed using Genespring (Agilent Technologies). Data was normalized

using RMA summarization without baseline transformation (normalized signal intensity, SI, given in Data S1B, C). Significantly different expression was determined by unpaired Mann-Whitney test with Benjamini-Hochberg correction ($p < 0.15$), and filtered for transcripts $\geq$ 2 fold different in all replicates. De-regulated transcripts were compared to those published as light-regulated and de-regulated in the *det1* and *pifq* mutants [8] using Access and Excel (Windows 10, Microsoft, Redmont, WA). A Parametric Analysis of Gene Set Enrichment (PAGE) analysis, which took into account both the number of entities and their respective expression patterns, was performed to determine GO terms enriched in the de-regulated genes using a Hochberg (FDR) multi-test adjustment and a significance of $p < 0.05$ [70].

Selected transcripts were validated in an independent experiment using qRT-PCR. For each genotype and condition, 120 to 150 seedlings were pooled per plate separately for each of three replicate petri plates and frozen directly in liquid nitrogen. RNA was extracted using TRIzol Reagent (Thermofisher Scientific, Schwerte, Germany), pooled in equal quantities from the replicates, and 800 ng RNA used in first strand cDNA synthesis using the SuperScript III kit and Oligo dT primer (Thermofisher Scientific, Schwerte, Germany). Four μL of a 1/30 dilution of the cDNA was used as template for qPCRs which were performed using a LightCycler 480 Real-Time PCR System (Roche Diagnostics, Mannheim, Germany) in 384-well plates. SYBR Green PCR Mastermix (Applied Biosystems Waltham, MA) was used to monitor amplification of cDNA using an annealing temperature of 60°C. Reactions with primer amplification efficiencies below 1.8 were discarded, and mean primer amplification efficiency (*PE*) for each primer pair calculated from all reactions. These were used with the individual Threshold Cycles (C_T) to calculate individual expression values (*Ev*) for each reaction $Ev = PE^{-CT}$. The mean *Ev* (*mEv*) for the housekeeper gene *UBQ10* (At4g05320) was used to calculate Relative Transcript Levels (RTLs) for each individual gene tested RTL (‰ *UBQ10*) = 1,000 · *Ev* / *mEv*(*UBQ10*), and the arithmetic mean and standard deviation of these RTLs was calculated from technical replicates. See Table S5 for primer sequences.

Confocal Microscopy

Dark- and light-grown *dez* seedlings homozygous for the *TBRgenomic::GFP* construct were incubated in 1 mM propidium iodide for 20 to 30 s, and imaged on a Leica SP5 confocal laser scanning microscope using a 40x PLAN APO water immersion lens, with excitation through the 488 nm laser and detection using eGFP and propidium iodide settings (Leica, Wetzlar, Germany).

μFTIR

Hypocotyls were embedded in OCT resin, followed by flash freezing in liquid-N_2-chilled isopentane. Transverse 20-μm sections were prepared using a cryo-microtome (Leica CM3050S, Wetzlar, Germany), freeze-dried and mounted on BaF_2 windows. Micro Fourier transformed Infra-Red (μFTIR) measurements were conducted at the European Synchrotron Radiation Facility (beamline ID21, ESRF, Grenoble, France). An IR microscope (Continuum, Thermo Nicolet, Madison, WI, USA) coupled to a FTIR spectrometer (Nexus, Thermo Nicolet) were used to collect spectra in reflection mode between 4,000 and 800 cm^{-1} with a 9 μm x 9 μm aperture. The IR microscope was equipped with a 32x objective, a motorized sample stage, and a liquid nitrogen-cooled 50 μm mercury cadmium telluride detector. Spectra were collected at a resolution of 6 cm^{-1} across entire sections, with 100 scans per pixel. Background spectra were collected every 30 min and used for automatic normalization. Data were extracted using OMNIC software (Thermo Fisher Scientific, Waltham, MA), baseline-corrected and the area corresponding to the epidermis was excluded from further analysis in order to avoid any signal arising from the non-penetrating resin used for embedding. The second derivative was taken of all spectra using the Savitzky-Golay algorithm and a 21-point window size [71], followed by scaling to 1. Scaled spectra were used for a principal component analysis (PCA), and the first five principal components (accounting for 82% of the total variation) were used as variables in a linear discriminant analysis (LDA) [72]. Statistical analysis were performed using the R statistical software [73], with the packages caret [74] and signal [75].

μXRF and μXANES

For the imaging of elemental distribution and Zn speciation in transverse sections of hypocotyls, cryo-microtome sections (thickness 35 μm) were deposited between two Ultralene foils before analysis on the microXAS beamline at the Swiss Light Source (SLS, Villigen, Switzerland). Elemental distribution was mapped by micro X-ray fluorescence (μXRF) in cryo-conditions (liquid nitrogen cryojet) using a 9.7 keV beam focused to 2 μm x 2 μm and a dwell time of 0.2 s. Micro X-ray absorption near edge structure (μXANES) spectra were recorded by scanning the Zn-absorption edge from 9500 to 9820 eV. A set of reference compound spectra was kindly provided by Dr. Géraldine Sarret: Zn^{2+}_{aq} (1 M $Zn(NO_3)_2$ solution), Zn(II)-citrate (10 mM $Zn(NO_3)_2$, 100 mM citrate, pH 4.5), Zn(II)-oxalate (33 mM $Zn(NO_3)_2$, 130 mM oxalate, pH 5.0), Zn(II)-organic acids (10 mM $Zn(NO_3)_2$, 33 mM malate, 33 mM citrate, 33 mM succinate, pH 5.5), Zn(II)-cell wall (1.4 μmol Zn g^{-1} DW bound to cell wall isolated from *Nicotiana tabacum* roots), Zn(II)-pectin (pectin containing 7.6 μmol Zn g^{-1} DW) [76]. In addition, the following reference spectra were recorded in this study: Zn(II)-histidine (10 mM $ZnCl_2$, 100 mM L-histidine, Sigma Chem., pH 6.0), Zn(II) cysteine in solution (Sigma-Aldrich Chemie), ZnS (solid salt, Sigma-Aldrich Chemie) and metallic Zn foil. Experimental μXANES spectra were first normalized, then modeled by Linear Combination Fitting (LCF) using the set of reference spectra listed above with Athena software [77]. A correction slope was allowed to compensate for small differences in data normalization, and no energy shift was allowed.

Electron Microscopy

Seven-day-old dark-grown wild-type and *dez* seedlings were cut at the midpoint of the hypocotyl and the middle of the cotyledon, then fixed in 0.1 M sodium cacodylate buffer (Plano, Wetzlar, Germany) at pH 6.9, containing 2.5% (w/v) glutaraldehyde (Plano,

Wetzlar, Germany), 2% (v/v) paraformaldehyde (EMS-CHEMIE, Gross-Umstadt, Germany) and 0.025% (w/v) $CaCl_2$ (Sigma, Steinheim, Germany) for 3 hr at RT, then overnight at 4°C. Samples were then rinsed 3 times in 0.1 M sodium cacodylate buffer, pH 6.9, at RT for 10 min, then incubated for 1 hr on ice in 0.1 M cacodylate buffer with 0.5% (w/v) OsO_4 (Plano, Wetzlar, Germany) and 0.15% (w/v) ferricyanide (Sigma, Steinheim, Germany). Samples were then rinsed 3 times in 0.1 M cacodylate buffer and 3 times in ultrapure water (Milli-Q, Merck, Darmstadt, Germany), 10 min per rinse. Samples were sequentially dehydrated in 25%, 50%, 75% and twice in 100% (v/v) ethanol at RT for 1 hr. Infiltration was performed at RT in 25% (v/v) LR White (EMS-CHEMIE, Gross-Umstadt, Germany) resin in ethanol overnight, all day in 50% (v/v) LR White in ethanol, overnight in 75% (v/v) LR White in ethanol, all day in 100% LR White. After another 48 hr in 100% LR White at 4°C, we embedded in 100% LR White at 100°C for 1.5 hr. After blocks had polymerized and cooled, they were trimmed with a Leica EM TRIM2 (Leica Histology and Microscopy, Wetzlar, Germany), and 90 nm sections were cut using a Leica EM UC7 Ultramicrotome and a Diatome Ultra diamond blade (Leica Histology and Microscopy, Wetzlar, Germany). Sections were placed on PLANO nickel grids (G2980N, EMS-CHEMIE, Gross-Umstadt, Germany) with a 2 mm x 1 mm slot per grid and a handle.

For immunolabeling [78], sections on grids were incubated with 60 μL goat serum buffer (a 1:20 dilution of goat serum in TRIS-buffered Saline (TBS) containing 1% (w/v) BSA) for 30 min at RT. This was followed by 3 incubations at RT for 10 min each with 50 μL blocking buffer (1x TBS with 1% (w/v) BSA). Each section was incubated at 4°C overnight in 14 μL of a 1:10 dilution of primary antibody (LM19 or LM20; Plant Probes, Leeds, UK) in blocking buffer, with shaking at 200 rpm and a lid cover to prevent evaporation. After 4 washes with 50 μL blocking buffer for 10 min each at RT, sections were shaken in 24 μL of a 1:20 dilution of secondary antibody (Anti-Rat IgG on 10-nm gold particles; PLANO, Wetzlar, Germany) in blocking buffer at 200 rpm at RT for 1 hr, followed by four 10 min washes in 50 μL blocking buffer, a rinse with MilliQ water and blotting dry. After an incubation in 2% (w/v) uranyl acetate for 6 min, followed by incubation with Reynolds lead citrate (Reynolds, 1963) for 6 min at RT, images were captured using a Zeiss Sigma VP with STEM detector at 20 kV with 30 μm aperture (Carl Zeiss AG, Jena, Germany).

Metal Analysis

Metal quantification was performed on 7-day-old dark-grown wild-type and *dez* seedlings cultivated on control and high-Zn media. Seedlings were either undesorbed (washed 3 times 10 min with ultrapure water) or desorbed (washed alternately for 10 min with ultrapure water, 10 mM EDTA pH 5.7, ultrapure water, 10 mM EDTA pH 5.7 and ultrapure water) on ice. Plant tissues were dried in an oven at 60°C for 3 d, allowed to equilibrate at room temperature for a further day. Plant tissues were weighed into acid-washed Duran glass tubes and mineralized upon addition of 2 mL 65% (w/w) HNO_3 at RT overnight and in a heating block at 80°C for 1 hr and at 120°C for 1.5 hr. Tubes were left to cool to below 50°C, and cleared by addition of 1 mL 30% (v/v) H_2O_2, kept at RT for 0.5 hr, 60°C for 0.5 hr, 100°C for 0.5 hr, left to cool to RT and subsequently filled up to a final volume of 10 mL with ultrapure water. Multi-element analysis of digests was conducted using Inductively-Coupled Plasma Optical Emission Spectrometry (ICP-OES) of these acid digests using an iCAPDuo 6500 instrument (Thermo Fisher Scientific, Dreieich, Germany), calibrated with a blank and a series of 5 multi-element standards manually pipetted from single-element standard solutions for 17 elements commonly detected in *A. thaliana* (AAS Standards, Bernd Kraft, Duisburg, Germany). Precision of measurements was validated by measurements of a sample blank and an intermediate calibration standard solution as well as a digest of a certified reference material (Virginia tobacco leaves, INCT-PVTL 6; Institute of Nuclear Chemistry and Technology, Warsaw, Poland) before and after each set of *ca*. 50 samples. Recoveries were (mean normalized to certified concentration ± relative standard deviation) 96% ± 5% for Ca and 92% ± 10% for Zn.

Preparation of Polygalacturonic Acid Digest

A solution of 10 mg mL^{-1} polygalacturonic acid (PGA; Sigma, Steinheim, Germany) was prepared in 50 mM sodium acetate (pH 5.5), 50 μg mL^{-1} Pectolyase Y-23 (Kyowa, Osaka, Japan) was added, and digestion was conducted at 30°C for 60 min. The reaction was stopped by incubation at 100°C for 5 min. Digests were spun down at 20,000x*g* for 10 min, and the supernatant collected and used to supplement plant growth media.

QUANTIFICATION AND STATISTICAL ANALYSIS

Each experiment was repeated two to five times independently, using 12 seeds per genotype and treatment. Poorly germinated seedlings or obvious phenotypic outliers were excluded from harvest and measurements. Data are shown for one representative of all experimental repeats, with n corresponding to the number of replicate seedlings used for the calculation of means ± SD. Statistical significance of differences between arithmetic means, unless stated otherwise, was assessed by Bonferroni-corrected Student's t tests ($p < 0.05$). Statistical analysis were performed using Excel (Microsoft). Data analysis for μFTIR, μXRF and μXANES were performed as described above.

DATA AND SOFTWARE AVAILABILITY

Microarray data are available under accession number GEO: GSE96589.